Cellular/Molecular

K_V7/M Channels Mediate Osmotic Modulation of Intrinsic Neuronal Excitability

Anna Caspi,[1] Felix Benninger,[1] and Yoel Yaari[1,2]

[1]Department of Medical Neurobiology, Institute for Medical Research Israel–Canada, The Hebrew University–Hadassah School of Medicine, Jerusalem 91120, Israel, and [2]The Interdisciplinary Center for Neuronal Computation, The Hebrew University, Jerusalem 91904, Israel

Modest decreases in extracellular osmolarity induce brain hyperexcitability that may culminate in epileptic seizures. At the cellular level, moderate hyposmolarity markedly potentiates the intrinsic neuronal excitability of principal cortical neurons without significantly affecting their volume. The most conspicuous cellular effect of hyposmolarity is converting regular firing neurons to burst-firing mode. This effect is underlain by hyposmotic facilitation of the spike afterdepolarization (ADP), but its ionic mechanism is unknown. Because blockers of K_V7 (KCNQ) channels underlying neuronal M-type K^+ currents (K_V7/M channels) also cause spike ADP facilitation and bursting, we hypothesized that lowering osmolarity inhibits these channels. Using current- and voltage-clamp recordings in CA1 pyramidal cells *in situ*, we have confirmed this hypothesis. Furthermore, we show that hyposmotic inhibition of K_V7/M channels is mediated by an increase in intracellular Ca^{2+} concentration via release from internal stores but not via influx of extracellular Ca^{2+}. Finally, we show that interfering with internal Ca^{2+}-mediated inhibition of K_V7/M channels entirely protects against hyposmotic ADP facilitation and bursting, indicating the exclusivity of this novel mechanism in producing intrinsic neuronal hyperexcitability in hyposmotic conditions.

Introduction

Reduction in plasma osmolarity associated with a wide range of clinical syndromes can lead to epileptic seizures (Andrew, 1991). Likewise, lowering extracellular osmolarity induces neuronal network hyperexcitability and epileptiform discharges in hippocampal slices (Andrew et al., 1989; Traynelis and Dingledine, 1989; Dudek et al., 1990; Ballyk et al., 1991; Saly and Andrew, 1993). These effects of hyposmolarity have been attributed mainly to enhanced excitatory electric field (ephaptic) effects and ionic interactions (e.g., increases in the extracellular concentration of K^+) consequent to cell swelling and concurrent shrinkage of the extracellular space (Traynelis and Dingledine, 1989; Ballyk et al., 1991). However, hyposmolarity was shown also to enhance the intrinsic excitability of principal hippocampal neurons. Thus, in CA1 pyramidal cells, lowering osmolarity markedly potentiated the spike afterdepolarization (ADP), causing regular firing neurons to convert to burst-firing mode (Azouz et al., 1997). Because bursting neurons play a pivotal role in neuronal recruitment and synchronization, this effect likely contributes to the hyposmotic enhancement of neuronal network excitability and induction of epileptic activity (Chagnac-Amitai and Connors, 1989; Jensen and Yaari, 1997; Sanabria et al., 2001; Yaari and Beck, 2002; Wittner and Miles, 2007; Yaari et al., 2007), yet the mechanisms responsible for hyposmotic spike ADP facilitation and bursting have not been elucidated.

The somatic spike ADP of adult CA1 pyramidal cells in normal physiological conditions is determined by interplay of two low voltage-activated, noninactivating currents in the perisomatic region: the persistent Na^+ current (I_{NaP}), which acts to redepolarize the neuron immediately after the fast spike (Azouz et al., 1996; Su et al., 2001; Yue et al., 2005), and the M-type K^+ current (I_M), which opposes I_{NaP} and repolarizes the neuron (Yue and Yaari, 2004, 2006). The latter current is generated by a subset of K_V7 (KCNQ) channels (K_V7/M channels) (Wang et al., 1998; Shah et al., 2002) that are subjected to modulation by many chemical transmitters (Brown and Yu, 2000). Voltage-gated Ca^{2+} currents flowing during the spike enhance the ADP, but this effect is exerted indirectly via intracellular block of K_V7/M channels, unleashing the depolarizing action of I_{NaP} (Chen and Yaari, 2008). Recently, we have shown that, in marked resemblance to the effects of lowering osmolarity, selective pharmacological blockage of K_V7/M channels strongly facilitates the spike ADP and induces bursting (Yue and Yaari, 2004, 2006). Given also that loss-of-function mutations in K_V7/M channels cause epileptic seizures in man (Charlier et al., 1998; Singh et al., 1998) and animals (Peters et al., 2005), this similarity raises the intriguing possibility that lowering osmolarity enhances intrinsic neuronal excitability by inhibiting K_V7/M channels. However, other mechanisms (e.g., hyposmotic enhancement of I_{NaP}) can be entertained.

Here we have used intracellular current- and voltage-clamp recordings techniques and pharmacological manipulations in hippocampal slices to clarify how lowering osmolarity facilitates

Received Feb. 25, 2009; revised June 18, 2009; accepted July 6, 2009.

This research was supported by the Binational United States–Israel Science Foundation, the Deutsche Forschungsgemeinschaft Sonderforschungsbereich TR3, the Henri J. and Erna D. Leir Chair for Research in Neurodegenerative Diseases, and the Humboldt Foundation [Feodor Lynen Research Fellowship (F.B.)].

Correspondence should be addressed to Dr. Yoel Yaari, Department of Medical Neurobiology, Institute for Medical Research Israel–Canada, Hebrew University–Hadassah School of Medicine, P.O. Box 12272, Jerusalem 91120, Israel. E-mail: yaari@md.huji.ac.il.

DOI:10.1523/JNEUROSCI.0942-09.2009

 0270-6474/09/2911098-14$15.00/0

the spike ADP and induces intrinsic bursting in CA1 pyramidal cells. Our data show that this hyposmotic action is mediated exclusively by inhibition of I_M via Ca^{2+} release from internal stores.

Materials and Methods

Hippocampal slice preparation. All animal experiments were conducted in accordance with the guidelines of the Animal Care Committee of the Hebrew University. Male Sabra rats (125–150 g) were decapitated under isoflurane anesthesia, and transverse hippocampal slices (400 μm) were prepared with a Leica VT1000S vibrating microslicer and transferred to a storage chamber perfused with oxygenated (95% O_2/5% CO_2) normosmotic artificial CSF (aCSF) at room temperature.

Solutions. Normosmotic (301 ± 0.7 mOsm; $n = 10$; measured with a Vapro-5520 vapor pressure osmometer; Wescor) aCSF contained the following (in mM): 100 NaCl, 3.5 KCl, 2 $MgCl_2$, 1.6 $CaCl_2$, 24 $NaHCO_3$, 10 D-glucose, and 60 mannitol. Moderately (240.8 ± 2.2 mOsm; $n = 5$; a 20% reduction) or mildly (270 ± 1.5 mOsm; $n = 5$; a 10% reduction) hyposmotic aCSFs were prepared by omitting all or 30 mM mannitol, respectively, so that ion concentrations and ionic strength of all aCSFs were the same. High K^+ aCSF was made by adding 26.5 mM KCl to normosmotic aCSF (final KCl concentration, 30 mM). The Ca^{2+}-free aCSF was prepared by replacing $CaCl_2$ with 2 mM $MgCl_2$. High Ca^{2+} aCSF was made by increasing $CaCl_2$ concentration to 3 mM. All aCSFs were titrated to pH 7.4. The aCSFs contained also the glutamate receptor antagonists 6-cyano-7-nitro-quinoxaline-2,3-dione (CNQX) (15 μM) and 2-amino-5-phosphono-valeric acid (50 μM) to block fast EPSPs and the $GABA_A$ receptor antagonist picrotoxin (100 μM) to block fast IPSPs. In experiments designed to measure membrane chord resistance (R_{chord}) or I_M, tetrodotoxin (TTX) (1 μM), Ni^{2+} (1 mM), and Cd^{2+} (300 μM) were added to the aCSFs after cell impalement to block voltage-gated Na^+ and Ca^{2+} channels, as well as Ca^{2+}-gated K^+ channels. Additional drugs used in specific experiments are indicated below.

Chemicals and drugs. All chemicals and drugs were purchased from Sigma, except for CNQX (Research Biochemicals), TTX (Alomone Labs), XE991 [10,10-bis(4-pyridinylmethyl)-9(10*H*)-anthracenone] and ZD7288 (4-ethylphenylamino-1,2-dimethyl-6-methylaminopyrimidinium chloride) (Tocris Bioscience), and retigabine (a kind gift from Valeant). Stock solutions (10 mM) of linopirdine and retigabine were prepared in ethanol and dimethylsulfoxide, respectively, and diluted 1:1000 when added to the aCSF. All other drugs were added to the aCSF from aqueous stock solutions. Measurements of drug effects were usually performed after 30 min of slice perfusion with the drug-containing aCSF.

Electrophysiological recordings. We used sharp glass microelectrodes filled with 3 M KCl (60–100 MΩ) and an Axoclamp 2B amplifier (Molecular Devices) for somatic intracellular recordings in the CA1 pyramidal layer. In some experiments, when indicated, 200 mM BAPTA was included in the microelectrode filling solution. The pyramidal cells included in this study had stable resting potentials more negative than −60 mV, apparent input resistances ≥25 MΩ, and overshooting action potentials. In current-clamp mode, the bridge balance was carefully monitored and adjusted before each measurement. Spikes were elicited by applying brief (4 ms) or long (180 ms) positive current pulses. In discontinuous voltage-clamp mode, the switching frequency between current injection and voltage sampling was 1.5–3.5 kHz. The current records were filtered at 0.3 kHz.

Measurement of membrane chord resistance (R_{chord}). For exploring modulation of R_{chord} by I_M modifying treatments, slices were superfused with aCSFs containing 1 μM TTX, 1 mM Ni^{2+}, and 300 μM Cd^{2+}. Injecting a series of five 0.9-s-long positive current ramps, increasing from 0 to 1 nA in increments of 200 pA, produced corresponding incremental depolarization ramps (see Fig. 4*Aa*). R_{chord} in the voltage range of I_M activation (greater than −60 mV) was measured from the slope of the second half of these voltage–current relationships.

Isolation and measurement of I_M. For pharmacological isolation of I_M, the slices were superfused with aCSFs containing 1 μM TTX, 10 μM retigabine, and 50 μM ZD7288. We used an established voltage protocol to elicit I_M in CA1 pyramidal cells (Halliwell and Adams, 1982; Schweitzer et al., 1990, 1998; Schweitzer, 2000). From a holding potential (V_h) of approximately −40 mV, seven or nine hyperpolarizing voltage steps (duration 0.9 s) incrementing by −5 or −6 mV, as indicated, were delivered. These steps induced slow current "relaxations" after the instantaneous inward current drops (see Fig. 5*Aa*), which represent the slow deactivation of I_M. Current relaxations were fitted by single-exponential curves (starting after the capacitance artifact) and were extrapolated back to the beginning of the hyperpolarizing command pulses. I_M amplitudes were derived as the differences between the instantaneous peak currents at command onset and the steady-state currents just before command offset.

Monitoring pyramidal cells size. We used a high-sensitivity cooled CCD camera (Nikon DS-Qi1) mounted on a Nikon Eclipse FN1 light microscope equipped with a 60× objective to visualize CA1 pyramidal cells *in situ*. The cell of interest was continuously monitored during exposure to the different aCSFs. In case of upward shifts attributable to swelling of the slice, the plane of focus was adjusted, keeping the maximum extent of the neuron visualized. The area in the visual field occupied by pyramidal cell soma (cross-sectional area) was measured by outlining the soma borders and integrating the enclosed area using NIS-Elements Advanced Research software (Nikon).

Data analysis. Offline analyses were performed with pClamp9 software (Molecular Devices). In current-clamp experiments, the size of the spike ADP was measured as the integrated "area under the curve" between the fast afterhyperpolarization (AHP) and the point at which membrane voltage returned to resting potential.

All results are presented as the mean ± SEM. Assessment of statistical significance of differences between means was performed with paired Student's *t* test or repeated-measures ANOVA, as appropriate.

Results

CA1 pyramidal cells do not swell in hyposmotic ACSF

Brain tissue swells under hyposmotic stress attributable to osmotic movement of water into the intracellular compartment (Somjen, 2004). However, recent studies suggest that cellular responses to low osmolarity are not uniform. In particular, it was found that neocortical pyramidal cells *in situ* (both *in vivo* and in neocortical slices) tenaciously maintain their volume when extracellular osmolarity is reduced by 40 mOsm (a 13.3% reduction in osmolarity) (Andrew et al., 2007; Risher et al., 2009). In contrast, astrocytes readily swell in this condition and remain hypovolemic for tens of minutes without displaying a regulatory volume decrease (Andrew et al., 1997; Risher et al., 2009).

To test how CA1 pyramidal cells *in situ* respond to a hyposmotic challenge, we monitored them visually during superfusion of hippocampal slices with moderately hyposmotic aCSF (−60 mOsm; a 20% reduction in osmolarity). Changes in soma volume were inferred from changes in maximal cross-sectional area of the soma (see Materials and Methods). A representative experiment is illustrated in Figure 1*A*. The neuron in the center of the microscope field was monitored starting 10 min before (Fig. 1*Aa*) until 30 min after changing from normosmotic to hyposmotic aCSF, and measurements were made at 5 min intervals (Fig. 1*Ab*). No significant change in soma cross-sectional area was evident during this observation period. Similar results were obtained in eight additional experiments, as summarized in Figure 1, *B* and *C* (cross-sectional area before and 30 min after changing to hyposmotic aCSF: 102.2 ± 5.8 and 101.8 ± 7.1 μm^2, respectively; $n = 9$). In contrast, raising K^+ concentration in the aCSF to 30 mM consistently caused a progressive increase in soma cross-sectional area, as illustrated in Figure 1, *D* and *E*. On average, high-K^+ aCSF caused an 18.5 ± 3.0% increase in soma cross-sectional area (before and 30 min after changing to high K^+

aCSF: 98.5 ± 6.9 and 122.2 ± 8.4 μm^2, respectively; $p < 0.05$; $n = 9$) (Fig. 1*F*).

These results suggest that, like their neocortical counterparts (Andrew et al., 2007; Risher et al., 2009), CA1 pyramidal cells do not swell in a hyposmotic milieu.

Hyposmolarity facilitates the ADP and induces bursting in CA1 pyramidal cells

In normosmotic aCSF, all impaled neurons ($n = 56$) fired a solitary spike followed by a distinct ADP when stimulated with brief (4 ms) positive current pulses (Fig. 2*Aa*) (Jensen et al., 1996). It was shown previously in these neurons that lowering osmolarity by 40 mOsm (a 13% decrease) facilitates the spike ADPs, causing many neurons (~43%) to fire high-frequency bursts of three to six spikes instead of solitary spikes (Azouz et al., 1997). Here we replicated these experiments using a stronger hyposmotic challenge (−60 mOsm; a 20% decrease). Changing to hyposmotic aCSF caused a slight depolarization of resting potential (from −66.7 ± 1.3 to −63.0 ± 1.5 mV; $n = 7$), which was counteracted by the injection of an appropriate steady negative current. A representative experiment is illustrated in Figure 2*A*. Lowering osmolarity steeply increased ADP size by 69.5 ± 7.2% (from 280.1 ± 28.5 to 477.0 ± 68.5 mV/ms) (Fig. 2*Ab*,*Ac* and overlaid traces in *Ae*). The facilitated ADP ultimately triggered three to five additional spikes, thus altering the firing mode of the neurons from regular to burst firing (Fig. 2*Ad*). Similar results were consistently obtained in all seven experiments, as summarized in Figure 2, *B* and *C*.

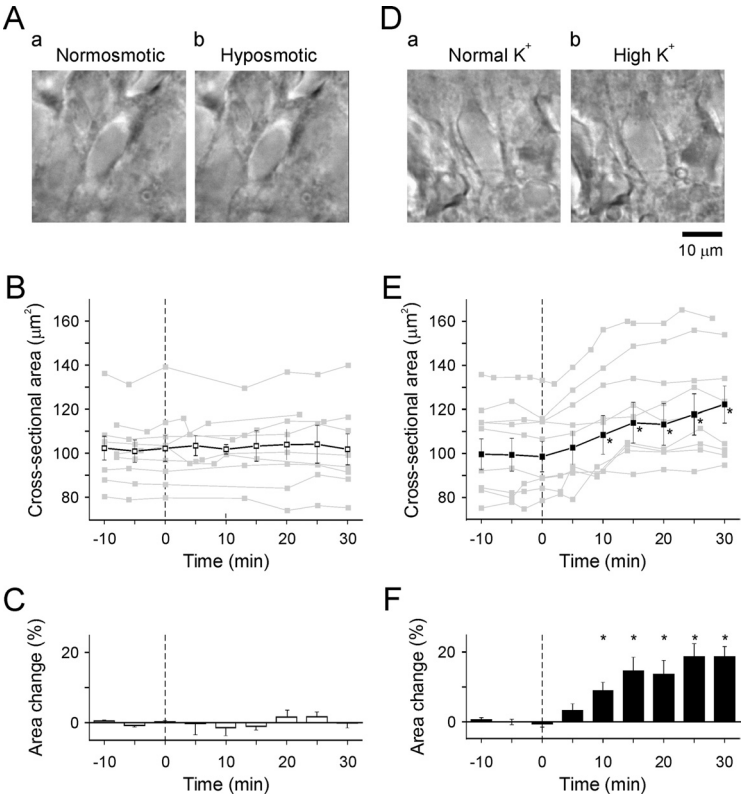

Figure 1. CA1 pyramidal cells do not swell in hyposmotic aCSF. ***A***, Images of a representative CA1 pyramidal cell (in the center of the visual field) monitored before (***a***) and 30 min after superfusion with hyposmotic (20% reduction) aCSF (***b***). Note no change in soma cross-sectional area. ***B***, Plots of maximal soma cross-sectional areas in nine neurons from separate experiments. Images were taken every 5 min, starting 10 min before and ending 30 min after changing from normosmotic to hyposmotic aCSF. The dark plot depicts the mean ± SEM values. ***C***, Summary histogram depicting the data in ***B*** as percentage changes in soma cross-sectional area. No significant changes were observed during the hyposmotic challenge. ***D***, Images of another neuron (in the center of the visual field) monitored before (***a***) and 30 min after superfusion with high-K^+ (30 mM) aCSF (***b***). Note expansion of cell size. ***E***, Plots of soma cross-sectional areas in nine neurons from separate experiments. Images were taken every 5 min, starting 10 min before and ending 30 min after changing from normal K^+ to high K^+ aCSF. The dark plot depicts the mean ± SEM values. ***F***, Summary histogram depicting the data in ***E*** as percentage changes in soma cross-sectional area. Significant increases in soma cross-sectional area were observed already 10 min after beginning the high K^+ challenge (*$p < 0.05$; $n = 9$).

The neurons were also stimulated with long (180 ms) depolarizing current pulses, incrementing in steps of 50 pA (up to 400 pA). The number of spikes evoked by each current step increased with stimulus intensity (Fig. 2*Da*,*E*). Lowering osmolarity enhanced spike output at all given intensities (Fig. 2*Db*,*E*) ($p < 0.05$; $n = 8$).

Hyposmotic bursting is driven by I_{NaP}

The spike ADP and associated bursting in adult CA1 pyramidal cells are normally driven by the depolarizing action of I_{NaP} (Azouz et al., 1996; Su et al., 2001; Yue et al., 2005). Direct potentiation of these potentials by Ca^{2+} currents was found during postnatal development (Magee and Carruth, 1999; Chen et al., 2005; Metz et al., 2005), during epileptogenesis (Sanabria et al., 2001; Su et al., 2002; Yaari et al., 2007), and after pharmacological blockage of A-type K^+ current in the apical dendrites (Magee and Carruth, 1999). To identify the inward currents driving hyposmotic bursting, we tested its sensitivity to Na^+ and Ca^{2+} channel blockers. In the case of I_{NaP}, we used the neuroprotective drug riluzole, which in CA1 pyramidal cells blocks I_{NaP} completely in doses that only mildly reduce transient Na^+ current (Yue et al., 2005). Adding 10 μM riluzole to the aCSF consistently abolished hyposmotic bursting, causing the neurons to fire single spikes in response to brief stimuli (Fig. 3*Aa–Ac*) ($p < 0.01$; $n = 11$). These results are summarized in the bar histogram shown in Figure 3*B*.

To test the potential contribution of Ca^{2+} currents, we used the Ca^{2+} channel blocker Ni^{2+}. Adding 1 mM Ni^{2+} to the aCSF (in replacement of 1 mM Mg^{2+}) enhanced hyposmotic bursting, eventually producing prolonged plateau potentials in all tested neurons (Fig. 3*Ca–Cc*) ($n = 6$). This effect most likely is attributable to blocking Ca^{2+}-gated K^+ currents generating the medium and slow AHPs (Madison and Nicoll, 1984; Storm, 1989). The prolonged bursts and plateau potentials produced in hyposmotic Ni^{2+}-containing aCSF were also converted to single spikes by subsequent addition of 10 μM riluzole (Fig. 3*Cd*). At a lower concentration of Ni^{2+} (100 μM) that preferentially blocks T-type and R-type Ca^{2+} currents (Lee et al., 1999; Williams et al., 1999) and suppresses T-type Ca^{2+} current-driven bursting (Su et al., 2002; Yaari et al., 2007), Ni^{2+} only slightly enhanced hyposmotic bursting (Fig. 3*Dab*) ($n = 2$).

Together, these findings indicate that hyposmotic bursting is driven predominantly by I_{NaP}, whereas Ca^{2+} currents limit burst duration likely by activating Ca^{2+}-gated K^+ currents.

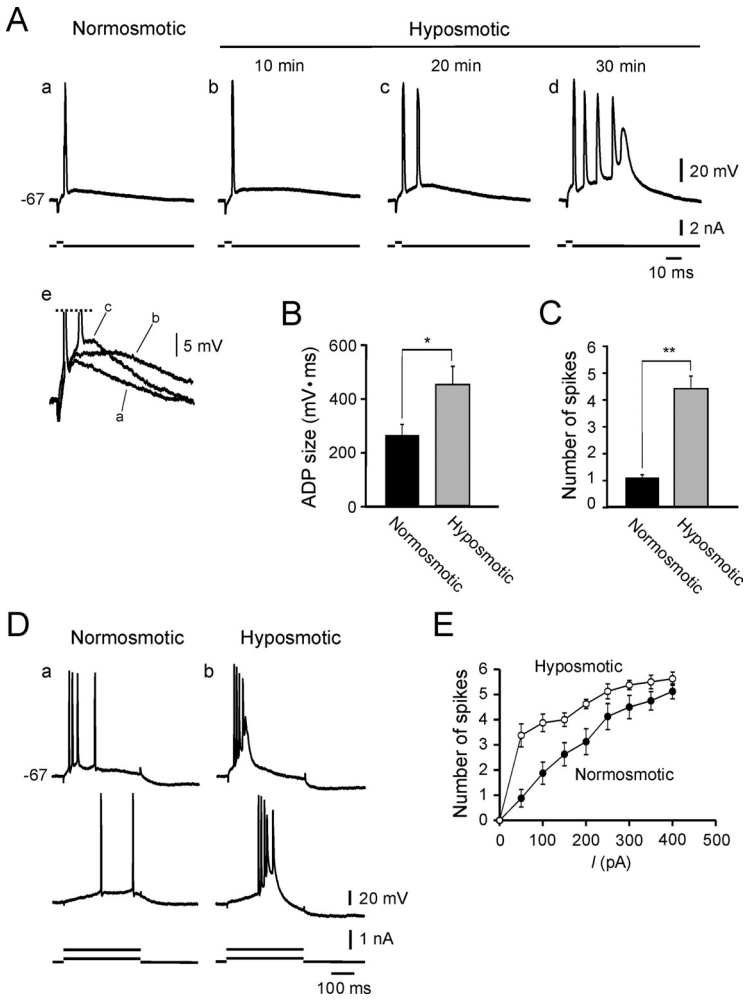

Figure 2. Hyposmolarity facilitates the spike ADP, induces bursting, and enhances spike output in CA1 pyramidal cells. In each panel showing current-clamp recordings, here and in all figures below, the bottom traces depict the injected current stimuli, and the top traces represent the recorded voltage responses. Resting potentials are depicted to the left of the voltage responses. The neurons were maintained at their native resting potential throughout the recording session by injecting appropriate direct current. ***A***, Lowering osmolarity by 20% caused progressive facilitation of the spike ADP and the conversion of the single spike responses to bursts of five spikes (***a–d***). Portions of traces in ***a–c*** are expanded and overlaid in ***e*** to allow comparison of the spike ADPs. ***B***, Bar histogram showing ADP size in normosmotic versus hyposmotic aCSFs ($n = 6$; $^*p < 0.05$). The ADPs were measured before the emergence of secondary spikes. ***C***, As in ***B*** but showing the number of spikes evoked by the brief stimuli ($n = 7$; $^{**}p < 0.01$). In hyposmotic aCSF, spike were counted after burst firing was established. ***D***, The neuron shown in ***A*** was also stimulated with a set of long (180 ms) depolarizing current pulses. Bottom traces depict the minimal spike responses (evoked by 100 pA in this case). Top traces show the responses to larger stimulus intensities (400 pA). Changing from normosmotic (***a***) to hyposmotic aCSF (***b***) increased spike frequency and spike output at all stimulus intensities. ***E***, Spike output plots showing the number of evoked spikes versus stimulus intensity in normosmotic (filled circles) and hyposmotic (open circles) aCSFs ($n = 8$; $p < 0.05$).

We first tested the hypothesis that hyposmotic facilitation of the spike ADP is attributable to inhibition of I_M. We began by monitoring R_{chord} in conditions of blocked voltage-gated Na^+ and Ca^{2+} currents and Ca^{2+}-gated K^+ currents (see Materials and Methods). To that end, the aCSFs contained 1 μM TTX, 1 mM Ni^{2+}, and 200 μM Cd^{2+}. The resting potential of the neurons in this series of experiments was -67.0 ± 1.3 mV ($n = 18$). In most neurons, the voltage ramp depolarizations evoked by the injected current ramps displayed a conspicuous delayed rectification (decrease in R_{chord} with depolarization), particularly at voltages above -60 mV (Fig. 4*Aa*). This rectification likely results from activation of I_M, whose threshold of activation is in this voltage range (Brown and Adams, 1980; Hu et al., 2007). Indeed, delayed rectification was reduced by the K_V7/M channel blocker XE991 (20 μM) (Fig. 4*Cab* and overlaid traced in *Cd*) and was accentuated by the K_V7/M channel enhancer retigabine (10 μM) (Fig. 4*Eab* and overlaid traces in *Ed*). In each tested neuron, we measured the average R_{chord} for the second half of the voltage–current relationship. XE991 increased R_{chord} by 120.7 $\pm$ 21.9% (from 13.6 $\pm$ 3.3 to 29.3 $\pm$ 4.3 MΩ; $n = 6$; $p < 0.05$; summary of results in Fig. 4*D*), whereas retigabine decreased R_{chord} by 59.9 $\pm$ 10.0% (from 8.2 $\pm$ 1.6 to 2.9 $\pm$ 0.9 MΩ; $n = 5$; $p < 0.05$) (summary of results in Fig. 4*F*).

In all tested neurons, lowering osmolarity mimicked the effect of XE991 in reducing delayed rectification (Fig. 4*Aa*,*Ab* and overlaid traces in *Ad*), causing R_{chord} to increase by 123.3 $\pm$ 35.0% (from 9.5 $\pm$ 1.7 to 23.8 $\pm$ 4.1 MΩ; $n = 8$; $p < 0.05$) (summary of results in Fig. 4*B*). This effect reversed during washing with normosmotic aCSF ($n = 3$) (Fig. 4*Ac* and overlaid traces in *Ad*; summary of results in *B*). Pretreatment of the neurons with XE991 (which by itself increased R_{chord}, as noted above) occluded this effect of hyposmolarity ($n = 5$) (Fig. 4*Cc* and overlaid traces in *Cd*; summary of results in *D*). Conversely, when R_{chord} was reduced by retigabine, changing to hyposmotic aCSF completely reversed its effect ($n = 5$) (Fig. 4*Ea–Ec* and overlaid traces in *Ed*; summary of results in *F*). These data strongly suggest that lowering osmolarity inhibits I_M.

Hyposmotic increase in membrane chord resistance

The growth of the spike ADP and conversion to bursting in hyposmotic aCSF may be attributable to a genuine increase in I_{NaP}. Alternatively, or additionally, it may result from a decrease in opposing K^+ currents. In CA1 pyramidal cells, the main K^+ current counteracting I_{NaP} and curtailing the spike ADP is I_M (Yue and Yaari, 2004). Inhibiting this current with K_V7/M channel blockers, such as linopirdine or XE991 (Aiken et al., 1995; Wang et al., 1998), was shown to facilitate the spike ADP and induce bursting in striking resemblance to the effects of low osmolarity. Likewise, bursts induced by inhibiting I_M were readily suppressed by inhibiting I_{NaP} with riluzole and markedly prolonged by blocking Ca^{2+} currents with 1 mM Ni^{2+} (Yue and Yaari, 2006).

Hyposmotic inhibition of I_M

We next examined the effects of lowering osmolarity on I_M directly, using the sharp microelectrode voltage-clamp technique (see Materials and Methods). The aCSFs in these experiments contained 1 μM TTX to block Na^+, 10 μM retigabine to enhance I_M (Tatulian et al., 2001), and 50 μM ZD7288 to eliminate activation of h-current at voltages below -70 mV (Halliwell and Ad-

ams, 1982; Gu et al., 2005). After impalement, the neurons were maintained at a holding potential (V_h) of -42.2 ± 0.37 mV ($n = 5$) to activate I_M and inactivate other classes of voltage-gated K^+ channels. Hyperpolarizing voltage steps (duration, 0.9 s; applied at 0.2 Hz) incrementing by -6 mV (down to approximately -96 mV) induced slow current relaxations after the instantaneous inward current drops (Fig. 5*Aa*). In each response, the current component undergoing relaxation represents the slow deactivation of I_M (Brown and Adams, 1980; Halliwell and Adams, 1982; Schweitzer et al., 1990, 1998; Schweitzer, 2000). The reversal potential of these currents was approximately -90 mV (Fig. 5*B*), approximating the reversal potential of K^+ (-96.4 ± 6.2 mV) (Jensen et al., 1993).

Hyposmotic aCSF reduced the holding current by $26.5 \pm 6.8\%$ (from 1.56 ± 0.07 to 1.14 ± 0.01 nA; $n = 5$) (Fig. 5*A*, dotted line). Concomitantly, the current relaxations were markedly reduced at all step potentials (Fig. 5*Ab*; the mean current–voltage relationship is depicted in *B*), indicating that I_M was inhibited. Thus, at -72 mV (Fig. 5*Aab*, bottom traces), I_M was inhibited by $71.0 \pm 8.9\%$ (from 118.0 ± 15.8 to 35.6 ± 11.9 pA; $n = 5$; $p < 0.05$) (Fig. 5*C*). All effects of hyposmotic aCSF on I_M reversed during restoring normal osmolarity (Fig. 5*Ac*) ($n = 2$). Adding 10 μM linopirdine to normosmotic aCSF decreased I_M by $64.8 \pm 17.4\%$ (from 64.2 ± 18.7 to 15.13 ± 13.6 pA; $n = 5$), thus mimicking the effects of hyposmolarity (Fig. 5*Ad*) ($n = 5$).

We tested also whether I_M is modified by a milder decrease in osmolarity, which may be more pertinent to physiological changes in osmolarity (Somjen, 2004). Reducing aCSF osmolarity by 30 mOsm (a 10% reduction) decreased I_M by $54.6 \pm 17.6\%$ (from 129.8 ± 15.8 to 61.5 ± 20.4 pA; $n = 5$; $p < 0.05$) (Fig. 5*C*).

In another series of experiments, we used the same voltage protocol and aCSF compositions described above to record I_M relaxations in CA1 pyramidal cells in two separate sets of slices: slices superfused with normosmotic aCSF ($n = 5$) and slices superfused with -20% (-60 mOsm) hyposmotic aCSF ($n = 5$). The mean holding potential in these experiments was -42.7 ± 0.39 mV ($n = 10$). Expectedly, as illustrated in Figure 5, *A* and *E*, I_M relaxations were much smaller in hyposmotic aCSF (Fig. 5*Ea*) than in normosmotic aCSF (Fig. 5*Da*). We then applied 20 μM XE991 to the aCSFs for up to 30 min to block I_M entirely. Application of XE991 reduced the holding current by $41.09 \pm 9.5\%$ (from 1.72 ± 0.15 to 1.01 ± 0.1 nA; $n = 5$; $p < 0.05$) in normosmotic aCSF and by $26.8 \pm 2.9\%$ (from 1.23 ± 0.03 to 0.90 ± 0.06 nA; $n = 5$; $p < 0.05$) in hyposmotic aCSF. No residual current relaxations were seen in XE991-treated neurons (Fig. 5*Db*,*Eb*). Subtracting the current traces obtained in XE991-containing aCSFs from the respective currents obtained before XE991 applications provided a set of pure I_M relaxations for each experimental condition (Fig. 5*Dc*,*Ec*). As shown in the mean current–voltage relationship in Figure 5*F*, I_M amplitudes recorded in hyposmotic aCSF were markedly smaller than those obtained in normosmotic aCSF at all step potentials. Thus, at a step potential of -72 mV, I_M in hyposmotic aCSF was $70.9 \pm 6.7\%$ smaller than in normosmotic aCSF (35.2 ± 6.5 vs 126.9 ± 7.5 pA, respectively; $n = 5$ in each group; $p < 0.01$) (Fig. 5*G*). This result is very consistent with the hyposmotic I_M inhibition estimated directly from I_M relaxations ($71.0 \pm 8.9\%$) (Fig. 5*C*).

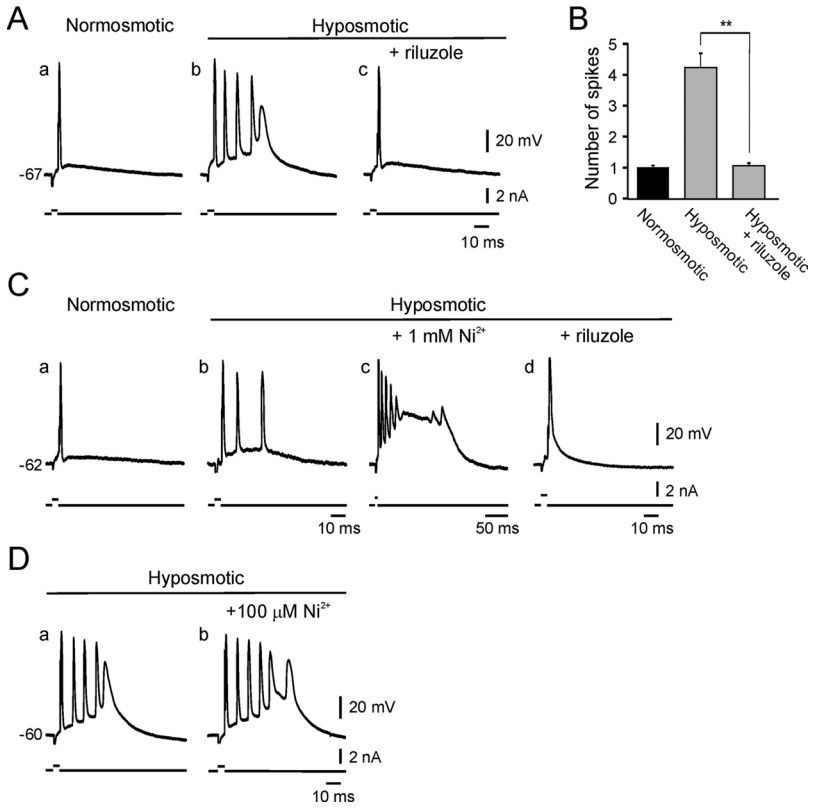

Figure 3. Hyposmotic bursting is driven by I_{NaP}. ***A***, In this neuron, lowering osmolarity by 20% invoked bursting (5 spikes; ***a***, ***b***), which was suppressed by adding the I_{NaP} blocker riluzole (10 μM) to the hyposmotic aCSF (***b***, ***c***). ***B***, Bar histogram summarizing the effects of riluzole on hyposmotic bursting ($n = 11$; $^{**}p < 0.01$). ***C***, In yet another neuron, hyposmotic bursting (***a***, ***b***) was markedly prolonged by the Ca^{2+} channel blocker Ni^{2+} (1 mM; $n = 6$; ***b***, ***c***). Again, 10 μM riluzole converted the prolonged bursts to single spikes (***c***, ***d***). ***D***, At a lower concentration (100 μM), Ni^{2+} only slightly increased the number of spikes in hyposmotic bursts ($n = 2$).

Hyposmotic I_M inhibition underlies ADP facilitation and induction of bursting

To examine whether the hyposmotic facilitation of the spike ADP and induction of bursting are exclusively or only partially attributable to I_M inhibition, we examined how lowering osmolarity affects neurons in which I_M was inhibited pharmacologically. Expectedly, pretreatment of the neurons with 20 μM XE991 in normosmotic aCSF converted single spikes to high-frequency bursts of three to six spikes (Yue and Yaari, 2004). To expose the underlying facilitated ADP, we suppressed the bursts by elevating extracellular Ca^{2+} concentration ($[Ca^{2+}]_o$) to 3 mM (Fig. 6*Aa*,*Ab*). The decreased excitability in high $[Ca^{2+}]_o$ is attributed to augmented screening of membrane surface potential by Ca^{2+} (Frankenhaeuser and Hodgkin, 1957; Su et al., 2001). A representative experiment is illustrated in Figure 6*A*. In high-Ca^{2+} aCSFs, lowering osmolarity failed to increase the spike ADP in this (Fig. 6*Ab*,*Ac* and overlaid traces in *Ad*), as well as in other four experiments ($n = 5$; $p > 0.05$) (Fig. 6*C*).

In another set of experiments, we suppressed XE991-induced bursting in normosmotic aCSF with 10 μM riluzole (Fig. 6*Bab*)

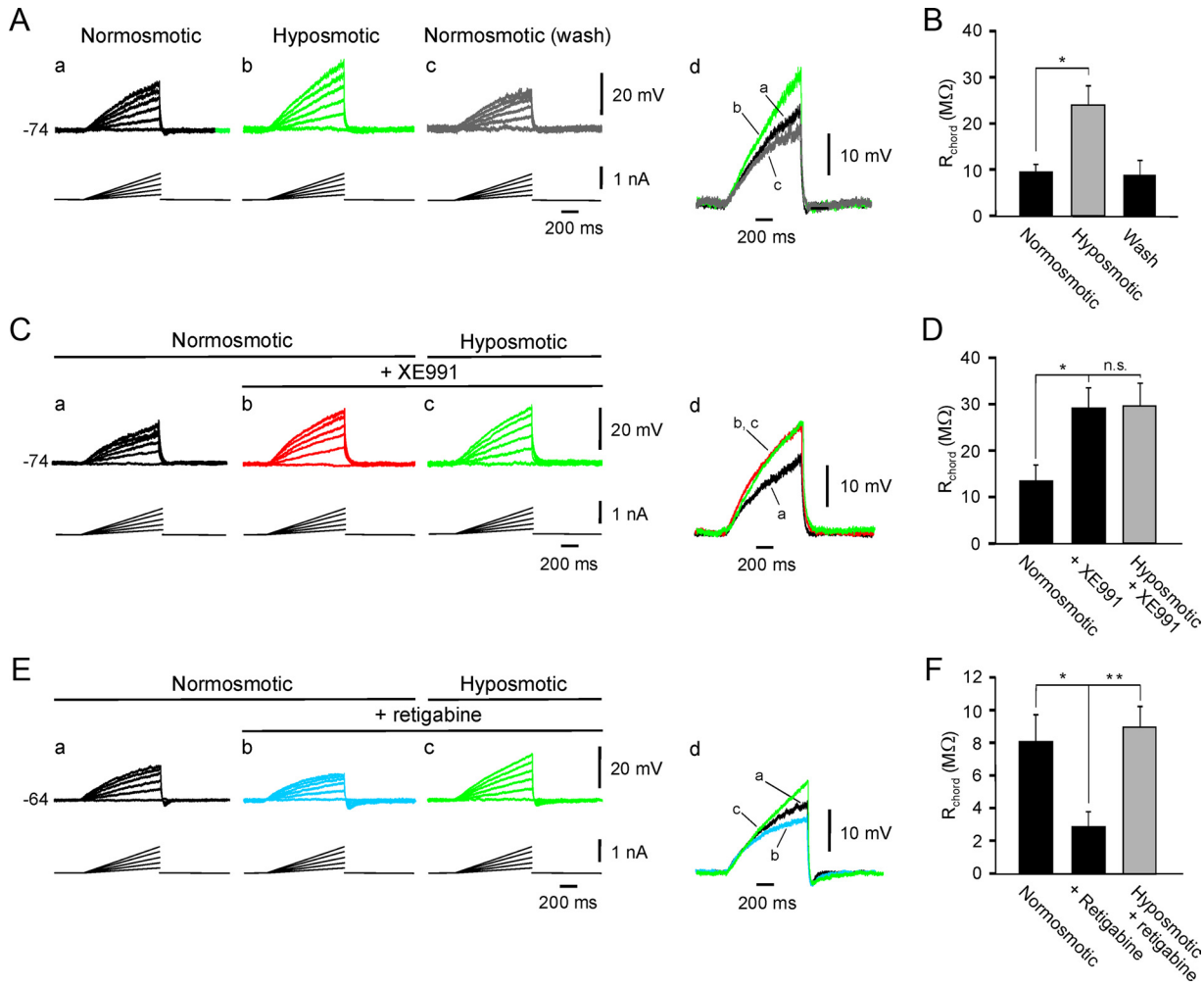

Figure 4. Hyposmotic modulation of membrane R_{chord}. Current-clamp recordings in aCSFs containing 1 μM TTX, 1 mM Ni^{2+}, and 300 μM Cd^{2+}. ***A***, In normosmotic aCSF, the neuron was injected with 0.9-s-long current ramps increasing up to 1 nA in steps of 200 pA. The depolarizing potentials evoked by the smaller ramps increased linearly, whereas those evoked by the larger ramps displayed delayed rectification, particularly during the second half of stimulation (***a***). Changing to hyposmotic aCSF (−20%) induced an increase in R_{chord} (***a***, ***b*** and overlaid traces in ***d*** depicting the responses to the largest ramp current). This effect reversed during restoring normal osmolarity (***b***, ***c*** and overlaid traces in ***d***). ***B***, Bar histogram summarizing the effects of lowering osmolarity on R_{chord} measured during the second half of the largest ramp current stimulus ($n = 8$; $^*p < 0.05$). ***C***, Adding XE991 (20 μM) to normosmotic aCSF also increased R_{chord} (***a***, ***b*** and overlaid traces in ***d***). Subsequent lowering of osmolarity had no additional effect on R_{chord} (***b***, ***c*** and overlaid traces in ***d***), indicating that blocking I_M occludes the effect of hyposmolarity. ***D***, Bar histogram summarizing the effects of XE991 and of lowering osmolarity in the presence of XE991 on R_{chord} ($n = 5$; $^*p > 0.05$). ***E***, Adding retigabine (10 μM) to normosmotic aCSF decreased R_{chord} (***a***, ***b*** and overlaid traces in ***d***). Changing to hyposmotic aCSF in the presence of retigabine reversed the effect of this drug and increased R_{chord} beyond control value (***b***, ***c*** and overlaid traces in ***d***). ***F***, Bar histogram summarizing the effects of retigabine ($n = 5$; $^*p < 0.05$) and hyposmolarity ($n = 5$; $^{**}p < 0.01$) on R_{chord}.

(Yue and Yaari, 2006). A representative experiment is illustrated in Figure 6*B*. In riluzole-containing aCSFs, lowering osmolarity again failed to further increase the spike ADP in this (Fig. 6*Bb*,*Bc* and overlaid traces in *Bd*), as well as in other four neurons ($n = 5$; $p > 0.05$) (Fig. 6*C*).

These data strongly suggest that I_M inhibition is the sole mechanism underlying hyposmotic ADP facilitation and bursting.

Intracellular Ca^{2+} release mediates hyposmotic increase in R_{chord}

In most cell types examined, hyposmotic swelling elicits an increase in intracellular Ca^{2+} concentration ($[Ca^{2+}]_i$) by enhancing Ca^{2+} influx and by releasing Ca^{2+} from internal stores (Lang et al., 1998; Pasantes-Morales and Morales Mulia, 2000). Both mechanisms reportedly contribute to the hyposmotic increase of $[Ca^{2+}]_i$ in dissociated hippocampal pyramidal cells, as well as in hippocampal slices (Borgdorff et al., 2000). As Ca^{2+} release from internal stores is a well characterized second-messenger cascade inhibiting K_V7/M channels (Delmas and Brown, 2005; Hernandez et al., 2008), we hypothesized that hyposmotic I_M inhibition may be mediated by an increase in $[Ca^{2+}]_i$.

To test this hypothesis, we first examined the effects of lowering osmolarity on R_{chord} in neurons injected with the fast Ca^{2+} chelator BAPTA. To that end, BAPTA (200 mM in the recording microelectrode) was injected by 100-ms-long negative current pulses (−500 pA) delivered at 3 Hz for at least 10 min. A representative experiment is illustrated in Figure 7*A*. Superfusing BAPTA-injected neurons with hyposmotic aCSF for up to 50 min consistently failed to change R_{chord} (Fig. 7*Aa*,*Ab* and overlaid traces in *Ad*). The same results were obtained in other six experiments ($n = 7$) (Fig. 7*C*), yet R_{chord} markedly increased with subsequent application of 20 μM XE991 ($n = 4$) (Fig. 7*Ab*,*Ac* and overlaid traces in *Ad*). These observations confirm that hyposmotic increase in R_{chord} is mediated by an increase in $[Ca^{2+}]_i$.

To assess the role of internal Ca^{2+} stores in the hyposmotic increase in R_{chord}, slices were preincubated for at least 30 min with the endoplasmic Ca^{2+}-ATPase inhibitor thapsigargin, known to deplete several types of internal Ca^{2+} stores (Thastrup et al., 1990; Takemura et al., 1991). As illustrated in Figure 7*B*, hyposmolarity failed to modify R_{chord} in this (Fig. 7*Ba*,*Bb* and overlaid traces in *Bd*), as well as in other four experiments ($n = 5$) (Fig. 7*C*), yet XE991 readily increased R_{chord} in the thapsigargin neurons ($n = 3$) (Fig. 7*Bb*,*Bc* and overlaid traces in *Bd*).

Together, these findings indicate that the augmentation of R_{chord} by low osmolarity requires Ca^{2+} release from internal stores.

Intracellular Ca^{2+} release mediates hyposmotic I_M inhibition

We next examined the consequences of BAPTA injection on hyposmotic inhibition of I_M. In five BAPTA-injected neurons, hyperpolarizing steps incrementing by −5 mV from a V_h of −44.2 ± 0.8 mV were applied to evoke I_M relaxations (Fig. 8*Aa*). Exposure of these neurons to hyposmotic aCSF for 40 min failed to modify I_M (Fig. 8*Ab*; the mean current–voltage relationship is shown in *B*).

In another set of experiments, we similarly examined the consequences of thapsigargin pretreatment on hyposmotic inhibition of I_M. The slices were preincubated for at least 30 min in aCSF containing 1 μM thapsigargin. In five neurons, slow I_M relaxations were elicited by hyperpolarizing steps of 5 mV from a V_h of 41.0 ± 1.0 mV (Fig. 8*Ca*). Exposure to hyposmotic aCSF for up to 40 min failed to modify I_M (Fig. 8*Cb*; the mean current–voltage relationship is shown in *D*).

Although these results strongly implicate Ca^{2+} release from internal stores in hyposmotic I_M inhibition, they do not exclude the participation of extracellular Ca^{2+} influx in this process, because Ca^{2+} release from internal stores may depend on Ca^{2+} influx (Chavis et al., 1996). The ramp stimulation experiments conducted in 1 mM Ni^{2+} and 300 μM Cd^{2+} containing aCSFs (Fig. 4) excluded a role for Ca^{2+} influx via voltage-gated channels. However, Ca^{2+} may enter through other routes, e.g., via TRPV4 channels that are Ca^{2+} permeable and open in hyposmotic aCSF (Liedtke et al., 2000, 2003). We therefore examined whether hyposmotic I_M inhibition persists in Ca^{2+}-free aCSFs. Slices were perfused with normosmotic Ca^{2+}-free aCSFs for at least 30 min. Slow I_M relaxations were elicited by hyperpolarizing steps of 5 mV from a V_h of 42.8 ± 0.5 mV ($n = 5$) (Fig. 8*Ea*). Changing to hyposmotic Ca^{2+}-free aCSF consistently caused I_M inhibition (Fig. 8*Eb*; the mean current–voltage relationship is shown in *F*). Thus, at −68 mV, I_M was inhibited by 63 ± 4% (from 129.7 ± 37.0 to 25.7 ± 7.0 pA; $n = 5$; $p < 0.05$). This is similar to hyposmotic inhibition of I_M in Ca^{2+}-containing aCSF (71 ± 8.9%) (Fig. 5*C*).

These three sets of results, summarized in Figure 8*G*, strongly indicate that Ca^{2+} release from internal stores mediates hyposmotic I_M inhibition regardless of extracellular Ca^{2+} influx.

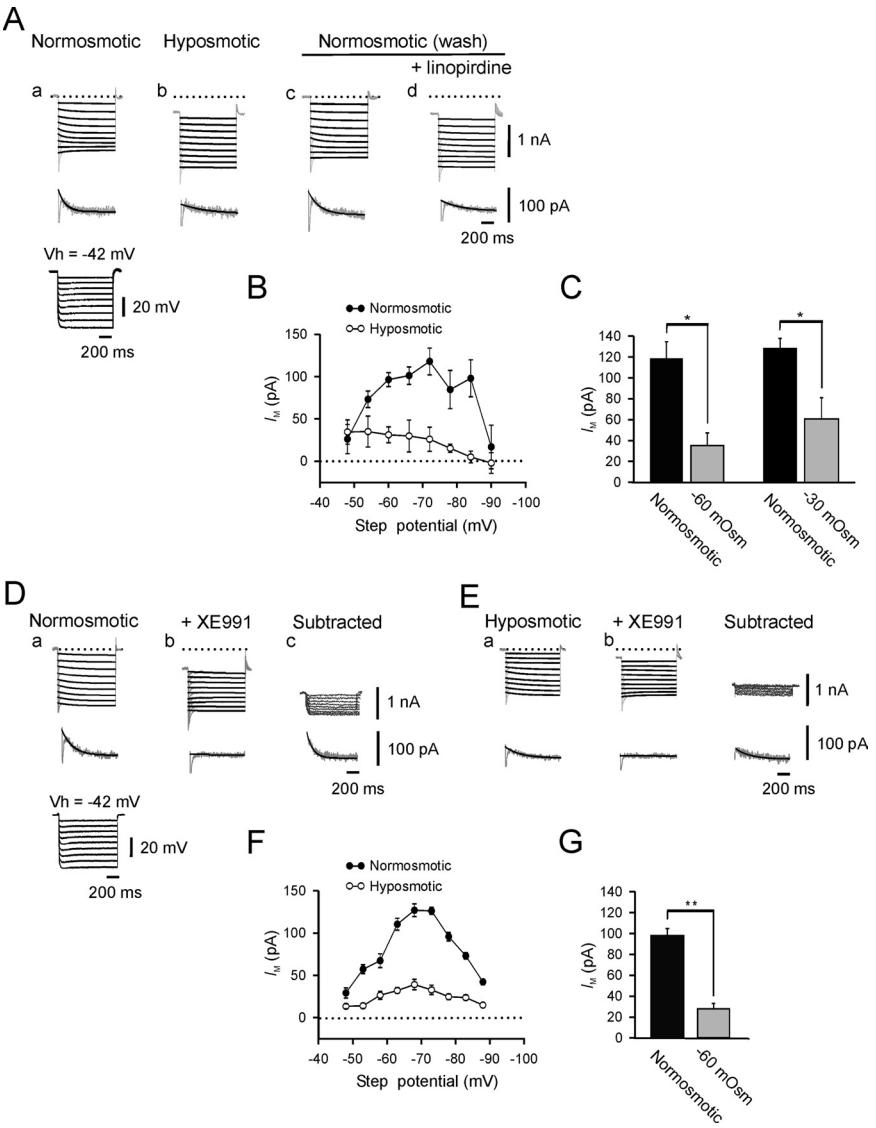

Figure 5. Lowering osmolarity inhibits I_M. Voltage-clamp recordings in aCSFs containing 1 μM TTX, 50 μM ZD7288, and 10 μM retigabine. ***A***, In this neuron, I_M amplitudes were measured from the outward current relaxations during nine sequential 0.9-s-long hyperpolarizing steps incrementing by −6 mV from a V_h of −42 mV (the voltage protocol is shown in ***a***, bottom). In ***a–d***, the top traces depict the responses to the voltage steps. Shown below is the current relaxation obtained by stepping to −72 mV together with the fitted monoexponential line that was extrapolated to the beginning of the voltage step. Changing to hyposmotic aCSF (−20%) markedly inhibited I_M (***a***, ***b***). This effect reversed completely after returning to normosmotic aCSF (***c***). Subsequent addition of 10 μM linopirdine to the normosmotic aCSF mimicked the effect of hyposmolarity in inhibiting I_M (***d***). ***B***, Plots of I_M amplitudes versus the hyperpolarizing command potentials in normosmotic (filled circles; $n = 5$) and hyposmotic (open circles; $n = 5$) aCSFs. ***C***, Bar histogram showing I_M inhibition by −20% (−60 mOsm) and −10% (−30 mOsm) reductions in osmolarity (*$p < 0.05$). ***D***, In another neuron superfused with normosmotic aCSF, I_M relaxations were recorded, as in ***A***, before (***a***) and after adding 20 μM XE991 to the aCSF to block I_M (***b***). The currents obtained after adding XE991 were subtracted from those obtained in control normosmotic aCSF (***c***). ***E***, Another neuron was superfused with −20% (−60 mOsm) hyposmotic aCSF. Again, I_M relaxations were recorded before (***a***) and after adding 20 μM XE991 to the aCSF (***b***). The currents obtained after adding XE991 were subtracted from those obtained in control hyposmotic aCSF (***c***). ***F***, Plots of XE991-sensitive current amplitudes versus the hyperpolarizing command potentials in normosmotic (filled circles; $n = 5$) and hyposmotic (open circles; $n = 5$) aCSFs. ***G***, Bar histogram comparing I_M amplitudes (obtained from XE991-sensitive current relaxations at −72 mV) in normosmotic versus hyposmotic aCSFs ($n = 5$; **$p < 0.01$).

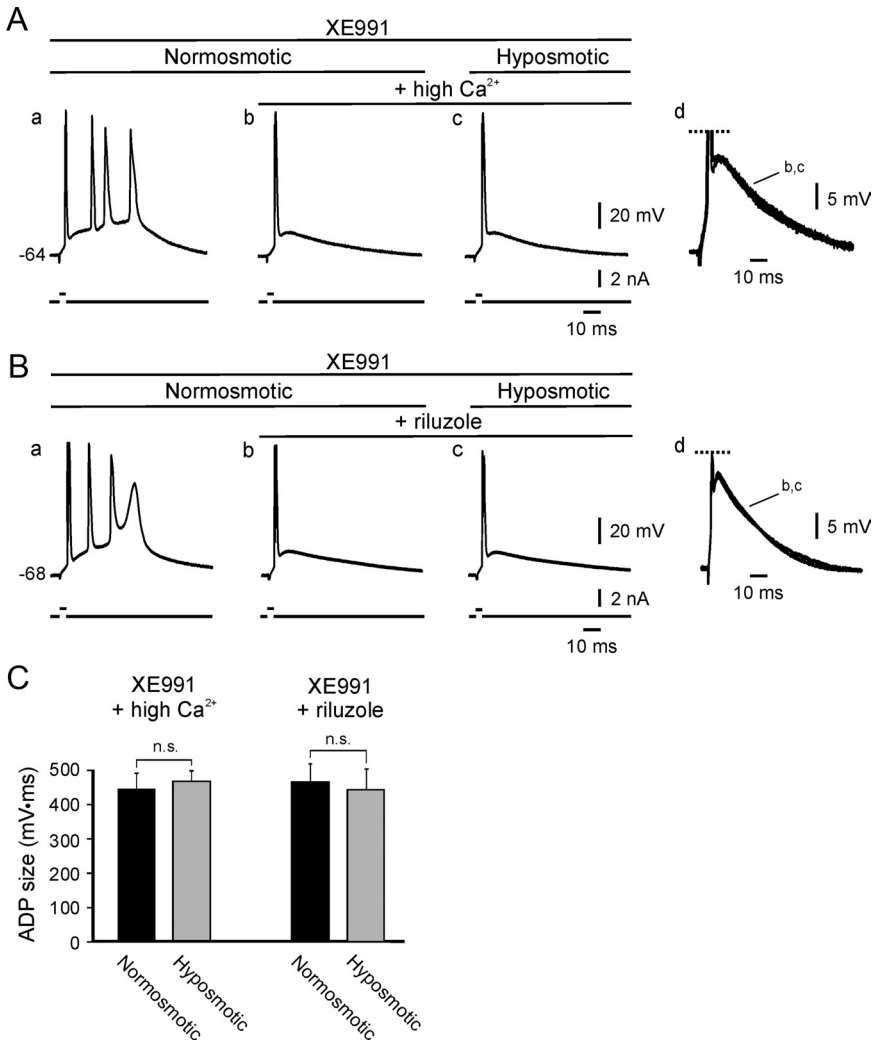

Figure 6. Blocking I_M pharmacologically occludes hyposmotic ADP facilitation. Current-clamp recordings of spike activity, as in Figure 1. ***A***, In the first neuron, adding 20 μM XE991 to normosmotic aCSF to block I_M induced bursting (***a***). The spike ADP was reduced by increasing aCSF Ca^{2+} content to 3 mM, converting bursting to single spiking (***b***). Reducing osmolarity of the high-Ca^{2+} aCSF had no effect on the spike ADP (***c*** and overlaid traces in ***d***). ***B***, In another neuron also converted to bursting by 20 μM XE991 in normosmotic aCSF (***a***), bursting was suppressed by adding 10 μM riluzole to the aCSF (***b***). Reducing osmolarity in this condition had no effect on the spike ADP (***c*** and overlaid traces in ***d***). ***C***, Bar histogram comparing ADP size in normosmotic versus hyposmotic aCSFs in XE991-treated neurons superfused with either high Ca^{2+} aCSF ($n = 5$; $p > 0.05$) or riluzole-containing aCSF ($n = 5$; $p > 0.05$).

Intracellular Ca^{2+} release mediates hyposmotic ADP facilitation and bursting

As a final assessment of the role of intracellular Ca^{2+} release in hyposmotic ADP facilitation and bursting, we examined the consequences of interfering with this process. Injecting BAPTA significantly reduced the spike ADP by 18.7 ± 4.5% (from 316.7 ± 30.3 to 253.2 ± 23.3 mV/ms; $n = 9$; $p < 0.01$) (Fig. 9*Aa*,*Ab* and overlaid traces in *Ad*), as reported recently (Chen and Yaari, 2008). However, the striking facilitatory effect of hyposmolarity on the ADP and bursting (Fig. 2*A*) was completely abolished in BAPTA-injected neurons [Fig. 9*Ab*,*Ac* and overlaid traces in *Ad* ($n = 9$; $p > 0.05$); summary of results in *B*]. To ensure that these results are not attributable to unspecific effects of BAPTA that may interfere with the propensity for bursting [e.g., enhancement of slow AHP current (Velumian and Carlen, 1999)], we also tested the effects of XE991 on BAPTA-injected neurons. Adding 20 μM XE991 to normosmotic aCSF facilitated the spike ADP to the point of bursting in the three tested neurons (Fig. 9*Ca–Cc*).

We next examined how thapsigargin affects the hyposmotic enhancement of intrinsic neuronal excitability. The slices were incubated with 1 μM thapsigargin for at least 30 min and then challenged with hyposmotic aCSF for 30 min or more. As illustrated in Figure 9*D*, hyposmotic ACSF had no effect on the spike ADP in thapsigargin-treated neurons [Fig. 9*Dab* and overlaid traces in *De* ($n = 5$; $p > 0.05$); data are summarized in *E*]. Notwithstanding, subsequent addition of 20 μM XE991 to the hyposmotic aCSF consistently caused ADP facilitation and bursting in the thapsigargin-treated neurons [Fig. 9*Dc*,*Dd* and overlaid traces in *De* ($n = 3$); summary of results in *E*].

Finally, we examined whether lowering osmolarity enhances intrinsic neuronal excitability in Ca^{2+}-free aCSF (Fig. 9*F*). Changing from normal to Ca^{2+}-free aCSF by itself caused spike ADP facilitation and bursting (Fig. 9*Da*,*Db*,*Fa*,*Fb*), as described previously (Su et al., 2001). The latter effect likely is attributable to enhancement of I_{NaP} by low extracellular Ca^{2+} (Yue et al., 2005), yet lowering osmolarity in Ca^{2+}-free aCSF caused a marked enhancement of burst discharge (in the neuron illustrated in Fig. 9*F*, lowering osmolarity increased the number of intraburst spikes from 3 to 11; *Fc*). Similar results were obtained in six experiments. These findings are consistent with previously reported ADP facilitation in 13%-reduced hyposmotic Ca^{2+}-free aCSF (Azouz et al., 1997).

Together, these data clearly demonstrate that hyposmotic facilitation of the spike ADP and induction of bursting are mediated exclusively by I_M inhibition via Ca^{2+} release from internal stores.

Discussion

In this study, we sought to identify the mechanism by which lowering osmolarity facilitates the spike ADP, converting single spikes to high-frequency spike bursts. We show that this mechanism involves hyposmotic release of Ca^{2+} from internal stores, leading to inhibition of I_M. Because I_M normally antagonizes the depolarizing action of I_{NaP}, its inhibition by low osmolarity unleashes I_{NaP}, causing the regenerative growth of the spike ADP to the point of bursting. The overall result is a marked increase in intrinsic neuronal excitability and spike output.

Hyposmolarity modifies CA1 pyramidal cell excitability without concurrent swelling

Recent studies strongly indicate that hyposmotic swelling of neocortical tissue is attributable mostly to water movement into astrocytes, whereas principal neurons are osmo-resistant (Andrew et al., 2007; Risher et al., 2009). The main reason for this disparity

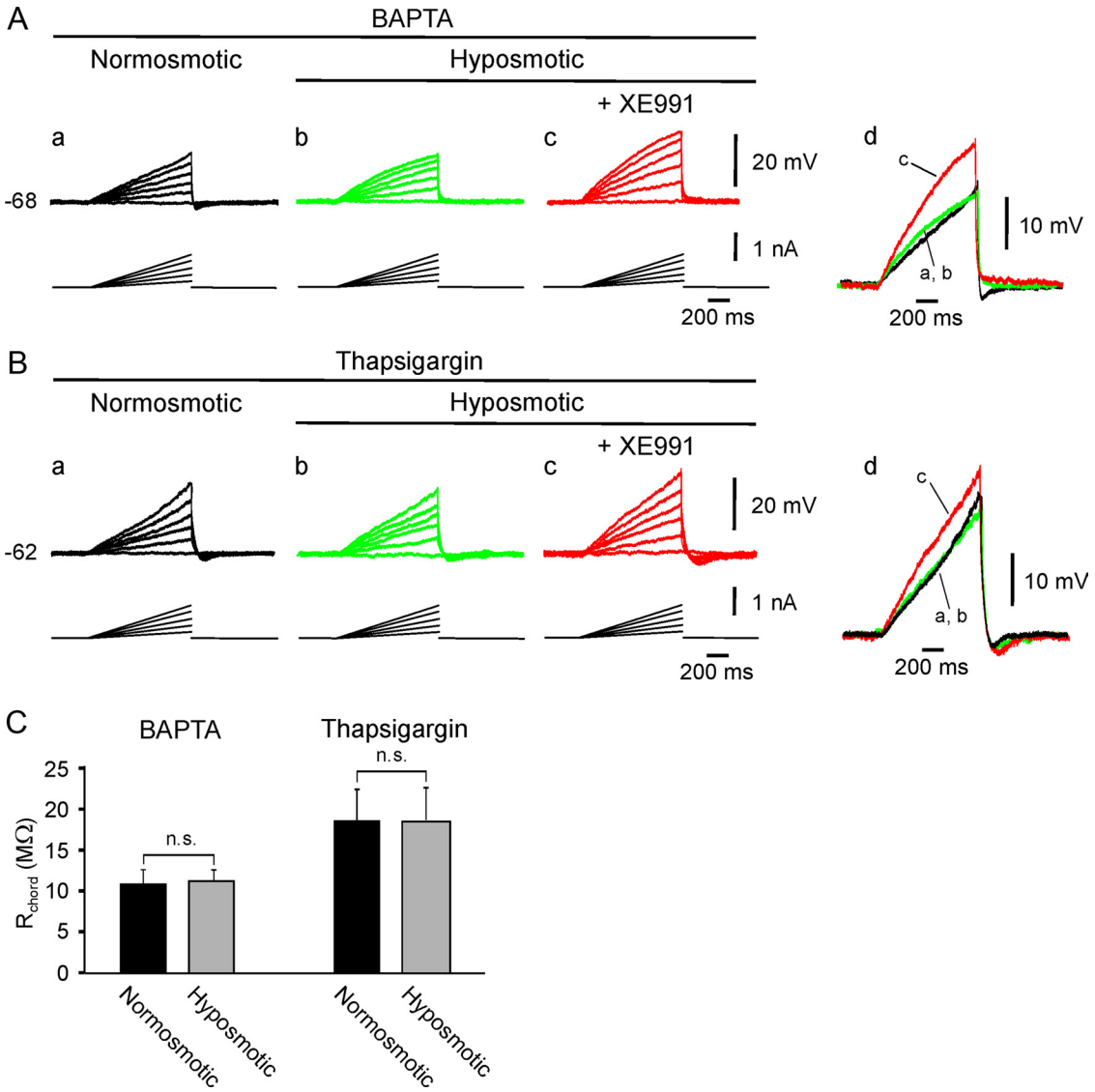

Figure 7. Preventing hyposmotic rise in $[Ca^{2+}]_i$ impedes hyposmotic enhancement of R_{chord}. Current-clamp recordings, as in Figure 2. ***A***, This neuron was filled with the fast Ca^{2+} chelator BAPTA during bath perfusion with normosmotic aCSF. Changing to hyposmotic aCSF had no significant effect on R_{chord} (***a***, ***b*** and overlaid traces in ***d***), yet adding 20 μM XE991 to the hyposmotic aCSF markedly increased R_{chord} (***c*** and overlaid traces in ***d***). ***B***, In another neuron pretreated with 1 μM thapsigargin (***a***), changing to hyposmotic aCSF also had no effect on the voltage responses to injected current ramps (***a***, ***b*** and overlaid traces in ***d***). Again, adding 20 μM XE991 to the hyposmotic aCSF markedly increased R_{chord} (***c*** and overlaid traces in ***d***). ***C***, Bar histogram comparing R_{chord} in normosmotic versus hyposmotic aCSFs in BAPTA-injected ($n = 7$; $p > 0.5$) and thapsigargin-treated ($n = 5$; $p > 0.05$) neurons.

is that astrocytes abundantly express aquaporins, whereas neurons lack these water-permeable channels (Nielsen et al., 1997). Our observations suggest that CA1 pyramidal cell somata also do not swell in hyposmotic aCSF (Fig. 1*Aab*) (Zhang and Bourque, 2003), likely because they also lack aquaporins (Nielsen et al., 1997). A recent study in neocortical slices has shown that axons and dendrites are also resistant to hyposmotic challenges (Andrew et al., 2007). Intriguingly, as in neocortical slices (Andrew et al., 2007), progressive swelling of CA1 pyramidal cell somata occurred in high K^+ aCSF (Fig. 1*Dab*). This effect may be attributed to water influx through nonaquaporin water conduits opened during prolonged depolarization (Andrew et al., 2007).

Despite the lack of osmotic swelling, CA1 pyramidal cells were strongly modified by hyposmotic aCSF. Lowering osmolarity caused ADP augmentation and bursting and increased overall spike output of these neurons. These changes likely are triggered by mechanical and/or chemical stimuli arising from the swelling of tissue surrounding the pyramidal cells.

Ionic mechanism of hyposmotic bursting

Facilitation of the spike ADP to the point of bursting occurs when the depolarizing action of perisomatic I_{NaP} (Yue and Yaari, 2006) or of dendritic Ca^{2+} currents (Magee and Carruth, 1999; Chen et al., 2005; Yaari et al., 2007) is enhanced attributable to increases in these currents and/or decreases in opposing K^+ currents. We found that hyposmotic bursting is readily suppressed by blocking I_{NaP}, whereas blockage of Ca^{2+} channels causes burst prolongation. The obvious conclusion is that hyposmotic bursting is driven predominantly by I_{NaP}, whereas recruitment of Ca^{2+} currents mediates burst termination likely by activating Ca^{2+}-gated K^+ currents (Golomb et al., 2006).

Inhibition of I_M underlies hyposmotic spike ADP facilitation and bursting

In CA1 pyramidal cells, the depolarizing action of I_{NaP} is antagonized mainly by I_M (Yue and Yaari, 2006). Therefore, I_{NaP}-driven bursting can result from an increase in I_{NaP} or, conversely,

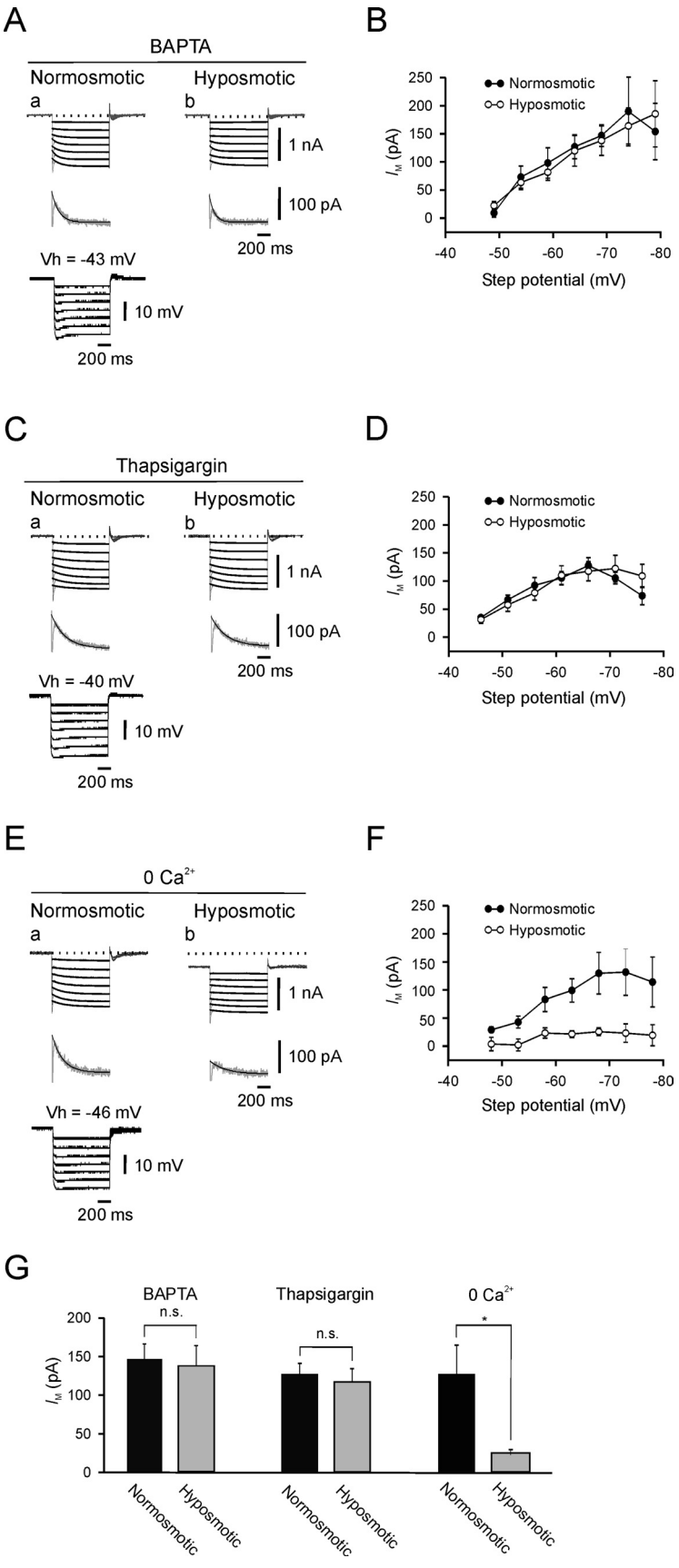

Figure 8. Intracellular Ca^{2+} release mediates hyposmotic I_M inhibition. Voltage-clamp recordings of I_M, as in Figure 3. ***A***, In this BAPTA-injected neuron, I_M amplitudes were measured from outward current relaxations during 900-ms-long hyperpolarizing steps incrementing by −5 mV from a V_h of −43 mV. Changing from normosmotic to hyposmotic aCSF had no effect on I_M (***a***, ***b***). ***B***, Plots of mean I_M amplitudes versus the hyperpolarizing command potentials in normosmotic (filled circles) and hyposmotic (open circles) aCSFs in BAPTA-injected neurons ($n = 5$; mean V_h of −44.2 ± 0.8 mV). The two current–voltage relationships are similar. ***C***, In a thapsigargin-treated neuron, I_M amplitudes were measured from outward current relaxations during 0.9-s-long hyperpolarizing steps incrementing by −5 mV from a V_h of −40 mV. Changing from normosmotic to hyposmotic aCSF had no effect on I_M (***a***, ***b***). ***D***, Plots of mean I_M amplitudes versus the hyperpolarizing command potentials in normosmotic (filled circles) and hyposmotic (open circles) aCSFs in thapsigargin-treated neurons ($n = 5$; mean V_h of 41 ± 1 mV). Again, the two current–voltage relationships are similar. ***E***, In a neuron bathed in Ca^{2+}-free aCSF, I_M amplitudes were measured from outward current relaxations during 0.9-s-long hyperpolarizing steps incrementing by −5 mV from a V_h of −46 mV. Changing from normosmotic to hyposmotic aCSF markedly suppressed I_M (***a***, ***b***). ***F***, Plots of mean I_M amplitudes versus the hyperpolarizing command potentials in normosmotic (filled circles) and hyposmotic Ca^{2+}-free (open circles; $n = 5$; mean V_h of −42.8 ± 0.48 mV) aCSFs. ***G***, Bar histogram comparing I_M amplitudes in normosmotic versus hyposmotic aCSFs in BAPTA-injected neurons (V_h of −69 mV; $n = 5$; $p > 0.05$), thapsigargin-treated neurons (V_h of −66 mV; $n = 5$; $p > 0.05$), and neurons superfused with Ca^{2+}-free aCSFs (V_h of −68 mV; $n = 5$; $^*p < 0.05$). Only in the latter condition lowering osmolarity reduced I_M (by 63 ± 4%).

from a decrease in I_M (Golomb et al., 2006). Our results strongly suggest that hyposmotic ADP facilitation and bursting is mediated by I_M inhibition rather than by I_{NaP} enhancement. First, lowering osmolarity inhibited I_M. Second, blocking I_M pharmacologically not only mimicked but also occluded all effects of hyposmolarity. Third, interfering with hyposmotic I_M inhibition by chelating intracellular Ca^{2+} or depleting internal Ca^{2+} stores protected against the hyposmotic effects. Together, these observations point to the critical and exclusive role of I_M inhibition in mediating hyposmotic enhancement of intrinsic neuronal excitability.

Role of internal Ca^{2+} stores

What mechanisms link hyposmolarity to I_M inhibition in CA1 pyramidal cells? Direct obstruction of K_V7/M channels via membrane tension associated with cell swelling is improbable for two reasons. First, these neurons do no swell in hyposmotic aCSF. Second, when $K_V7.2$ and $K_V7.3$ subunits (the main constituents of K_V7/M channels) (Wang et al., 1998; Shah et al., 2002) are coexpressed with aquaporins in *Xenopus* oocytes, they are resistant to osmotic swelling of these cells (Grunnet et al., 2003). Therefore, an intracellular signaling cascade likely mediates hyposmotic inhibition of these channels. In CA1 pyramidal cells, lowering osmolarity was shown to increase $[Ca^{2+}]_i$ by enhancing Ca^{2+} influx and Ca^{2+} release from internal

stores (Borgdorff et al., 2000). In the same neurons, Ca^{2+} influx during single spikes was shown to inhibit K_V7/M channels, causing significant spike ADP facilitation (Selyanko and Sim, 1998; Chen and Yaari, 2008). Furthermore, K_V7/M channels in excised inside-out patches from sympathetic neurons were directly inhibited by Ca^{2+} with an IC_{50} of ~100 nM (Selyanko and Brown, 1996). This inhibition is mediated by calmodulin bound to the C-terminal domain of K_V7/M subunits (Yus-Najera et al., 2002; Gamper and Shapiro, 2003; Gamper et al., 2005; Shahidullah et al., 2005). We therefore hypothesized that lowering osmolarity inhibits I_M by elevating $[Ca^{2+}]_i$. In support of our hypothesis, we found that injection of the fast Ca^{2+} chelator BAPTA prevents hyposmotic I_M inhibition. Furthermore, we found that hyposmotic I_M inhibition persists in Ca^{2+}-free aCSF but is abolished by depleting internal Ca^{2+} stores with thapsigargin. Together, these findings strongly indicate that hyposmotic I_M inhibition is achieved by the release of internally stored Ca^{2+} into the cytoplasm with subsequent block of K_V7/M channels.

Our results do not illuminate the precise mechanisms by which hyposmolarity triggers the release of internally stored Ca^{2+} in pyramidal cells. Lowering osmolarity enhances the release of multiple transmitters from neurons (Schousboe and Pasantes-Morales, 1992) and glia (Darby et al., 2003; Takano et al., 2005), some of which inhibit I_M by releasing Ca^{2+} from IP_3-sensitive stores in the endoplasmic reticulum (Delmas and Brown, 2005). However, hyposmotic release of internally stored Ca^{2+} was observed also in dissociated CA1 pyramidal cells devoid of contacts with other neurons or glia (Borgdorff et al., 2000), as well as in many cell types other than neurons (Fischer et al., 1997; Missiaen et al., 1997). Thus, the nature of the physicochemical mechanisms coupling extracellular hyposmolarity to Ca^{2+} release from internal stores remains to be identified.

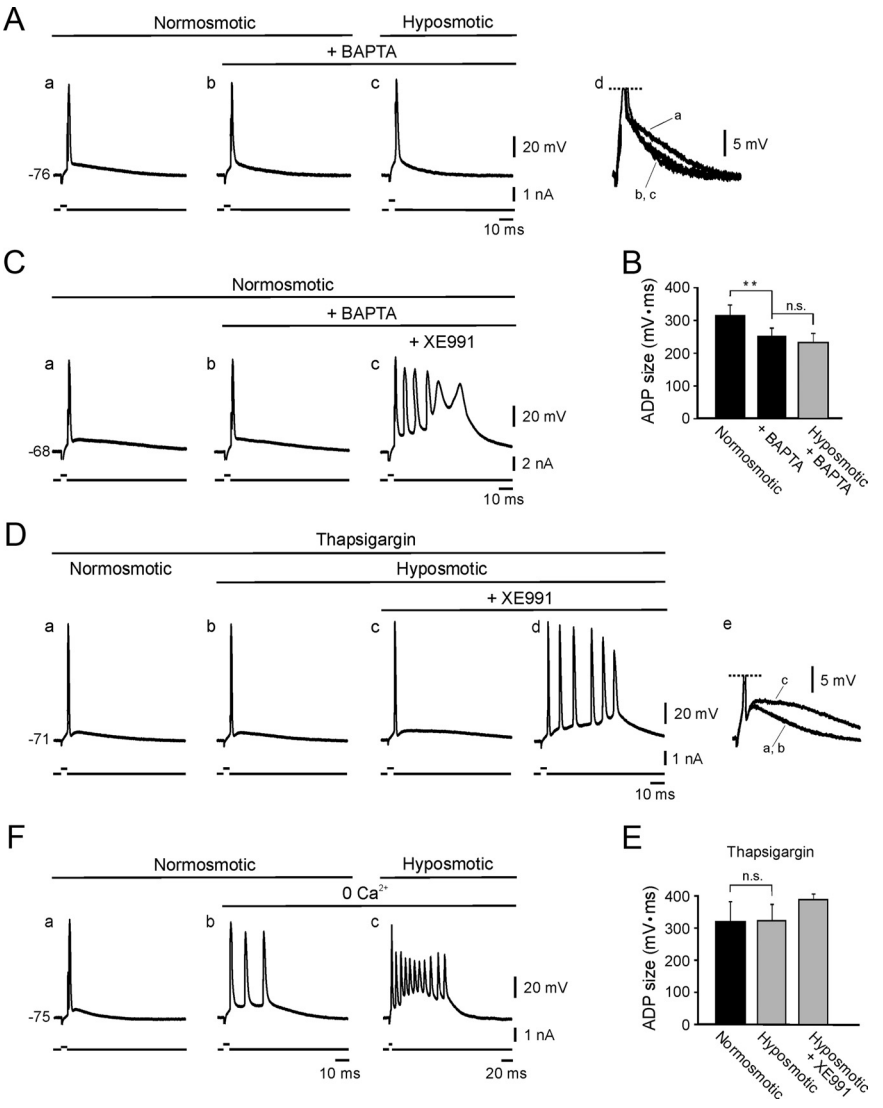

Figure 9. Intracellular Ca^{2+} release mediates hyposmotic ADP facilitation and bursting. Current-clamp recordings of spike activity, as in Figure 1. ***A***, In this neuron bathed in normosmotic aCSF, BAPTA injection suppressed the spike ADP (***a***, ***b*** and overlaid traces in ***d***). In nine similar experiments, BAPTA-injection reduced ADP size by 18.7 ± 4.5% ($p < 0.01$). Changing to hyposmotic aCSF had no effect on ADP size in the representative neurons (***c*** and overlaid traces in ***d***), as well as in all other BAPTA-injected neurons ($n = 9$; $p > 0.05$). ***B***, Bar histogram summarizing the experiments illustrated in ***A*** (**$p < 0.01$). ***C***, In another BAPTA-injected neuron (***a***, ***b***), blocking I_M with 20 μM XE991 facilitated the spike ADP to the point of bursting. Similar results were obtained in another two neurons. ***D***, In this neuron pretreated with 1 μM thapsigargin, changing from normosmotic to hyposmotic aCSF had no effect on the spike ADP (***a***, ***b*** and overlaid traces in ***e***). Adding 20 μM XE991 to the hyposmotic aCSF caused ADP facilitation to the point of bursting (***c***, ***d*** and overlaid traces in ***e***). ***E***, Bar histogram showing ADP sizes in thapsigargin-treated neurons in normosmotic and hyposmotic aCSFs ($n = 5$; $p > 0.05$) and after XE991 application ($n = 3$). ***F***, Another neuron was bathed with Ca^{2+}-free normosmotic aCSF, which by itself caused ADP facilitation to the point of bursting (***a***, ***b***). Changing to Ca^{2+}-free hyposmotic aCSF caused marked enhancement of bursting. Similar results were obtained in six similar experiments.

An increase in $[Ca^{2+}]_i$ is expected not only to block K_V7/M channels but also to activate Ca^{2+}-gated K^+ channels, an effect that would tend to oppose I_M inhibition and suppress intrinsic neuronal excitability. However, in hippocampal neurons, the Ca^{2+} sensitivities of large-conductance (BK) Ca^{2+}-gated K^+ channels (EC_{50} of 2–4 μM) (Smart, 1987; Franciolini, 1988; Gong et al., 2001) and of small-conductance (SK) Ca^{2+}-gated K^+ channels (EC_{50} of 0.6 μM) (Hirschberg et al., 1999) are considerably smaller than that of K_V7/M channels (EC_{50} of 100–120 nM) (Selyanko and Brown, 1996; Selyanko and Sim, 1998). Therefore, a hyposmotic increase in $[Ca^{2+}]_i$ to ~150 nM, as measured in acutely dissociated pyramidal cells (Borgdorff et al., 2000), may inhibit K_V7/M channels without concurrently activating BK or SK channels. It is also possible that Ca^{2+} released from internal stores by hyposmotic stimulation is spatially targeted to a specific microdomain of K_V7/M channels (Delmas and Brown, 2002). It is noteworthy that K_V7/M controlling the spike ADP and bursting are localized to the axon initial segment (Devaux et al., 2004; Yue and Yaari, 2006; Shah et al., 2008), which has not been shown to express any type of Ca^{2+}-gated K^+ channels.

Functional implications

Small changes (1–3%) in brain osmolarity accompany normal activity and play an integral part in the control of brain-fluid

homeostasis (Bourque, 2008). Reductions in osmolarity ≥10% used in this study are more relevant to pathophysiological conditions of impaired renal water excretion or excessive water intake, in which serum osmolarity can decrease to 230 mOsm (Adrogué and Madias, 2000; Verbalis, 2003). The clinical manifestations of these disorders are primarily neurological, including grand mal seizures (Andrew, 1991). Hyposmotic seizures and seizure-like discharges occur also in experimental animals and in brain tissue *in vitro*. They have been attributed mainly to enhanced nonsynaptic excitatory interactions consequent to cell swelling (Andrew et al., 1989; Traynelis and Dingledine, 1989; Dudek et al., 1990; Ballyk et al., 1991; Saly and Andrew, 1993). Here we provide an alternate or complementary mechanism: hyposmotic I_M inhibition. Several lines of evidence indicate that I_M inhibition strongly enhances brain excitability. First, mutations in $K_V7.2$ and $K_V7.3$ K^+ channel genes leading to reductions in I_M cause neonatal seizures (Charlier et al., 1998; Singh et al., 1998). Likewise, conditional transgenic suppression of $K_V7.2$ channels in mouse brain produces an epileptic phenotype (Peters et al., 2005). Finally, blocking K_V7/M channels with linopirdine or XE991 induces epileptiform seizures (Qiu et al., 2007), whereas enhancing K_V7/M channel activity with retigabine exerts an anti-seizure action (Armand et al., 1999, 2000; Dost and Rundfeldt, 2000).

The cellular mechanisms by which I_M inhibition causes neuronal network hyperexcitability likely include the induction of intrinsic bursting in principal neurons (Yue and Yaari, 2004), as well as reduction in early spike frequency adaptation (Gu et al., 2005; Otto et al., 2006). Furthermore, inhibiting I_M presynaptically enhances the release of neurotransmitters (Peretz et al., 2007) and postsynaptically augments the temporal summation of EPSPs (Hu et al., 2007). All these effects would summate to enhance the frequency, spread, and synchronization of neuronal spike discharge, leading to epileptic seizures. Given that hyposmotic I_M inhibition can be easily prevented (e.g., by pharmacological interference with the release of internally stored Ca^{2+}), it would be important to determine in the future whether averting this effect of hyposmolarity exerts an anti-seizure effect in experimental and clinical hyposmotic conditions.

References

Adrogué HJ, Madias NE (2000) Hypernatria. N Engl J Med 342:1581–1589.

Aiken SP, Lampe BJ, Murphy PA, Brown BS (1995) Reduction of spike frequency adaptation and blockade of M-current in rat CA1 pyramidal neurones by linopirdine (DuP 996), a neurotransmitter release enhancer. Br J Pharmacol 115:1163–1168.

Andrew RD (1991) Seizure and acute osmotic change: clinical and neurophysiological aspects. J Neurol Sci 101:7–18.

Andrew RD, Fagan M, Ballyk BA, Rosen AS (1989) Seizure susceptibility and the osmotic state. Brain Res 498:175–180.

Andrew RD, Lobinowich ME, Osehobo EP (1997) Evidence against volume regulation by cortical brain cells during acute osmotic stress. Exp Neurol 143:300–312.

Andrew RD, Labron MW, Boehnke SE, Carnduff L, Kirov SA (2007) Physiological evidence that pyramidal neurons lack functional water channels. Cereb Cortex 17:787–802.

Armand V, Rundfeldt C, Heinemann U (1999) Effects of retigabine (D-23129) on different patterns of epileptiform activity induced by 4-aminopyridine in rat entorhinal cortex hippocampal slices. Naunyn Schmiedebergs Arch Pharmacol 359:33–39.

Armand V, Rundfeldt C, Heinemann U (2000) Effects of retigabine (D-23129) on different patterns of epileptiform activity induced by low magnesium in rat entorhinal cortex hippocampal slices. Epilepsia 41:28–33.

Azouz R, Jensen MS, Yaari Y (1996) Ionic basis of spike after-depolarization and burst generation in adult rat hippocampal CA1 pyramidal cells. J Physiol 492:211–223.

Azouz R, Alroy G, Yaari Y (1997) Modulation of endogenous firing patterns by osmolarity in rat hippocampal neurones. J Physiol 502:175–187.

Ballyk BA, Quackenbush SJ, Andrew RD (1991) Osmotic effects on the CA1 neuronal population in hippocampal slices with special reference to glucose. J Neurophysiol 65:1055–1066.

Borgdorff AJ, Somjen GG, Wadman WJ (2000) Two mechanisms that raise free intracellular calcium in rat hippocampal neurons during hypoosmotic and low NaCl treatment. J Neurophysiol 83:81–89.

Bourque CW (2008) Central mechanisms of osmosensation and systemic osmoregulation. Nat Rev Neurosci 9:519–531.

Brown BS, Yu SP (2000) Modulation and genetic identification of the M channel. Prog Biophys Mol Biol 73:135–166.

Brown DA, Adams PR (1980) Muscarinic suppression of a novel voltage-sensitive K^+ current in a vertebrate neuron. Nature 283:673–676.

Chagnac-Amitai Y, Connors BW (1989) Synchronized excitation and inhibition driven by intrinsically bursting neurons in neocortex. J Neurophysiol 62:1149–1162.

Charlier C, Singh NA, Ryan SG, Lewis TB, Reus BE, Leach RJ, Leppert M (1998) A pore mutation in a novel KQT-like potassium channel gene in an idiopathic epilepsy family. Nat Genet 18:53–55.

Chavis P, Fagni L, Lansman JB, Bockaert J (1996) Functional coupling between ryanodine receptors and L-type calcium channels in neurons. Nature 382:719–722.

Chen S, Yaari Y (2008) Spike Ca^{2+} influx upmodulates the spike afterdepolarization and bursting via intracellular inhibition of K_V7/M channels. J Physiol 586:1351–1363.

Chen S, Yue C, Yaari Y (2005) A transitional period of Ca^{2+}-dependent spike afterdepolarization and bursting in developing rat CA1 pyramidal cells. J Physiol 567:79–93.

Darby M, Kuzmiski JB, Panenka W, Feighan D, MacVicar BA (2003) ATP released from astrocytes during swelling activates chloride channels. J Neurophysiol 89:1870–1877.

Delmas P, Brown DA (2002) Junctional signaling microdomains: bridging the gap between the neuronal cell surface and Ca^{2+} stores. Neuron 36:787–790.

Delmas P, Brown DA (2005) Pathways modulating neural KCNQ/M (K_V7) potassium channels. Nat Rev Neurosci 6:850–862.

Devaux JJ, Kleopa KA, Cooper EC, Scherer SS (2004) KCNQ2 is a nodal K^+ channel. J Neurosci 24:1236–1244.

Dost R, Rundfeldt C (2000) The anticonvulsant retigabine potently suppresses epileptiform discharges in the low Ca^{2+} and low Mg^{2+} model in the hippocampal slice preparation. Epilepsy Res 38:53–66.

Dudek FE, Obenaus A, Tasker JG (1990) Osmolality-induced changes in extracellular volume alter epileptiform bursts independent of chemical synapses in the rat: importance of non-synaptic mechanisms in hippocampal epileptogenesis. Neurosci Lett 120:267–270.

Fischer R, Schliess F, Häussinger D (1997) Characterization of the hypoosmolarity-induced Ca^{2+} response in cultured rat astrocytes. Glia 20:51–58.

Franciolini F (1988) Calcium and voltage dependence of single Ca^{2+}-activated K^+ channels from cultured hippocampal neurons of rat. Biochim Biophys Acta 943:419–427.

Frankenhaeuser B, Hodgkin AL (1957) The action of calcium on the electrical properties of squid axons. J Physiol 137:218–244.

Gamper N, Shapiro MS (2003) Calmodulin mediates Ca^{2+}-dependent modulation of M-type K^+ channels. J Gen Physiol 122:17–31.

Gamper N, Li Y, Shapiro MS (2005) Structural requirements for differential sensitivity of KCNQ K^+ channels to modulation by Ca^{2+}/calmodulin. Mol Biol Cell 16:3538–3551.

Golomb D, Yue C, Yaari Y (2006) Contribution of persistent Na^+ current and M-type K^+ current to somatic bursting in CA1 pyramidal cells: combined experimental and modeling study. J Neurophysiol 96:1912–1926.

Gong LW, Gao TM, Huang H, Tong Z (2001) Properties of large conductance calcium-activated potassium channels in pyramidal neurons from the hippocampal CA1 region of adult rats. Jpn J Physiol 51:725–731.

Grunnet M, Jespersen T, MacAulay N, Jørgensen NK, Schmitt N, Pongs O, Olesen SP, Klaerke DA (2003) KCNQ1 channels sense small changes in cell volume. J Physiol 549:419–427.

Gu N, Vervaeke K, Hu H, Storm JF (2005) Kv7/KCNQ/M and HCN/h, but not KCa2/SK channels, contribute to the somatic medium after-hyperpolarization and excitability control in CA1 hippocampal pyramidal cells. J Physiol 566:689–715.

Halliwell JV, Adams PR (1982) Voltage-clamp analysis of muscarinic excitation in hippocampal neurons. Brain Res 250:71–92.

Hernandez CC, Zaika O, Tolstykh GP, Shapiro MS (2008) Regulation of neural KCNQ channels: signalling pathways, structural motifs and functional implications. J Physiol 586:1811–1821.

Hirschberg B, Maylie J, Adelman JP, Marrion NV (1999) Gating properties of single SK channels in hippocampal CA1 pyramidal neurons. Biophys J 77:1905–1913.

Hu H, Vervaeke K, Storm JF (2007) M-channels (Kv7/KCNQ channels) that regulate synaptic integration, excitability, and spike pattern of CA1 pyramidal cells are located in the perisomatic region. J Neurosci 27:1853–1867.

Jensen MS, Yaari Y (1997) Role of intrinsic burst firing, potassium accumulation, and electrical coupling in the elevated potassium model of hippocampal epilepsy. J Neurophysiol 77:1224–1233.

Jensen MS, Cherubini E, Yaari Y (1993) Opponent effects of potassium on GABAA-mediated postsynaptic inhibition in the rat hippocampus. J Neurophysiol 69:764–771.

Jensen MS, Azouz R, Yaari Y (1996) Spike after-depolarization and burst generation in adult rat hippocampal CA1 pyramidal cells. J Physiol 492:199–210.

Lang F, Busch GL, Völkl H (1998) The diversity of volume regulatory mechanisms. Cell Physiol Biochem 8:1–45.

Lee JH, Gomora JC, Cribbs LL, Perez-Reyes E (1999) Nickel block of three cloned T-type calcium channels: low concentrations selectively block $\alpha 1_H$. Biophys J 77:3034–3042.

Liedtke W, Choe Y, Martí-Renom MA, Bell AM, Denis CS, Sali A, Hudspeth AJ, Friedman JM, Heller S (2000) Vanilloid receptor-related osmotically activated channel (VR-OAC), a candidate vertebrate osmoreceptor. Cell 103:525–535.

Liedtke W, Tobin DM, Bargmann CI, Friedman JM (2003) Mammalian TRPV4 (VR-OAC) directs behavioral responses to osmotic and mechanical stimuli in *Caenorhabditis elegans*. Proc Natl Acad Sci U S A 100 [Suppl 2]:14531–14536.

Madison DV, Nicoll RA (1984) Control of the repetitive discharge of rat CA1 pyramidal neurones in vitro. J Physiol 354:319–331.

Magee JC, Carruth M (1999) Dendritic voltage-gated ion channels regulate the action potential firing mode of hippocampal CA1 pyramidal neurons. J Neurophysiol 82:1895–1901.

Metz AE, Jarsky T, Martina M, Spruston N (2005) R-type calcium channels contribute to afterdepolarization and bursting in hippocampal CA1 pyramidal neurons. J Neurosci 25:5763–5773.

Missiaen L, De Smedt H, Parys JB, Sipma H, Maes K, Vanlingen S, Sienaert I, Van Driessche W, Casteels R (1997) Synergism between hypotonically induced calcium release and fatty acyl-CoA esters induced calcium release from intracellular stores. Cell Calcium 22:151–156.

Nielsen S, Nagelhus EA, Amiry-Moghaddam M, Bourque C, Agre P, Ottersen OP (1997) Specialized membrane domains for water transport in glial cells: high-resolution immunogold cytochemistry of aquaporin-4 in rat brain. J Neurosci 17:171–180.

Otto JF, Yang Y, Frankel WN, White HS, Wilcox KS (2006) A spontaneous mutation involving Kcnq2 (Kv7.2) reduces M-current density and spike frequency adaptation in mouse CA1 neurons. J Neurosci 26:2053–2059.

Pasantes-Morales H, Morales Mulia S (2000) Influence of calcium on regulatory volume decrease: role of potassium channels. Nephron 86:414–427.

Peretz A, Sheinin A, Yue C, Degani-Katzav N, Gibor G, Nachman R, Gopin A, Tam E, Shabat D, Yaari Y, Attali B (2007) Pre- and post-synaptic activation of M-channels by a novel opener dampens neuronal firing and transmitter release. J Neurophysiol 97:283–295.

Peters HC, Hu H, Pongs O, Storm JF, Isbrandt D (2005) Conditional transgenic suppression of M channels in mouse brain reveals functions in neuronal excitability, resonance and behavior. Nat Neurosci 8:51–60.

Qiu C, Johnson BN, Tallent MK (2007) K^+ M-current regulates the transition to seizures in immature and adult hippocampus. Epilepsia 48:2047–2058.

Risher WC, Andrew RD, Kirov SA (2009) Real-time passive volume responses of astrocytes to acute osmotic and ischemic stress in cortical slices and in vivo revealed by two-photon microscopy. Glia 57:207–221.

Saly V, Andrew RD (1993) CA3 neuron excitation and epileptiform discharge are sensitive to osmolality. J Neurophysiol 69:2200–2208.

Sanabria ER, Su H, Yaari Y (2001) Initiation of network bursts by Ca^{2+}-dependent intrinsic bursting in the rat pilocarpine model of temporal lobe epilepsy. J Physiol 532:205–216.

Schousboe A, Pasantes-Morales H (1992) Role of taurine in neural cell volume regulation. Can J Physiol Pharmacol [Suppl] 70:S356–S361.

Schweitzer P (2000) Cannabinoids decrease the K^+ M-current in hippocampal CA1 neurons. J Neurosci 20:51–58.

Schweitzer P, Madamba S, Siggins GR (1990) Arachidonic acid metabolites as mediators of somatostatin-induced increase of neuronal M-current. Nature 346:464–467.

Schweitzer P, Madamba SG, Siggins GR (1998) Somatostatin increases a voltage-insensitive K^+ conductance in rat CA1 hippocampal neurons. J Neurophysiol 79:1230–1238.

Selyanko AA, Brown DA (1996) Intracellular calcium directly inhibits potassium M channels in excised membrane patches from rat sympathetic neurons. Neuron 16:151–162.

Selyanko AA, Sim JA (1998) Ca^{2+}-inhibited non-inactivating K^+ channels in cultured rat hippocampal pyramidal neurones. J Physiol 510:71–91.

Shah MM, Mistry M, Marsh SJ, Brown DA, Delmas P (2002) Molecular correlates of the M-current in cultured rat hippocampal neurons. J Physiol 544:29–37.

Shah MM, Migliore M, Valencia I, Cooper EC, Brown DA (2008) Functional significance of axonal Kv7 channels in hippocampal pyramidal neurons. Proc Natl Acad Sci U S A 105:7869–7874.

Shahidullah M, Santarelli LC, Wen H, Levitan IB (2005) Expression of a calmodulin-binding KCNQ2 potassium channel fragment modulates neuronal M-current and membrane excitability. Proc Natl Acad Sci U S A 102:16454–16459.

Singh NA, Charlier C, Stauffer D, DuPont BR, Leach RJ, Melis R, Ronen GM, Bjerre I, Quattlebaum T, Murphy JV, McHarg ML, Gagnon D, Rosales TO, Peiffer A, Anderson VE, Leppert M (1998) A novel potassium channel gene, KCNQ2, is mutated in an inherited epilepsy of newborns. Nat Genet 18:25–29.

Smart TG (1987) Single calcium-activated potassium channels recorded from cultured rat sympathetic neurones. J Physiol 389:337–360.

Somjen GG (2004) Osmotic stress and the brain. Ions in the brain: normal function, seizures and stroke, pp 63–73. New York: Oxford UP.

Storm JF (1989) An after-hyperpolarization of medium duration in rat hippocampal pyramidal cells. J Physiol 409:171–190.

Su H, Alroy G, Kirson ED, Yaari Y (2001) Extracellular calcium modulates persistent sodium current-dependent burst-firing in hippocampal pyramidal neurons. J Neurosci 21:4173–4182.

Su H, Sochivko D, Becker A, Chen J, Jiang Y, Yaari Y, Beck H (2002) Upregulation of a T-type Ca^{2+} channel causes a long-lasting modification of neuronal firing mode after status epilepticus. J Neurosci 22:3645–3655.

Takano T, Kang J, Jaiswal JK, Simon SM, Lin JH, Yu Y, Li Y, Yang J, Dienel G, Zielke HR, Nedergaard M (2005) Receptor-mediated glutamate release from volume sensitive channels in astrocytes. Proc Natl Acad Sci U S A 102:16466–16471.

Takemura H, Ohshika H, Yokosawa N, Oguma K, Thastrup O (1991) The thapsigargin-sensitive intracellular Ca^{2+} pool is more important in plasma membrane Ca^{2+} entry than the IP_3-sensitive intracellular Ca^{2+} pool in neuronal cell lines. Biochem Biophys Res Commun 180:1518–1526.

Tatulian L, Delmas P, Abogadie FC, Brown DA (2001) Activation of expressed KCNQ potassium currents and native neuronal M-type potassium currents by the anti-convulsant drug retigabine. J Neurosci 21:5535–5545.

Thastrup O, Cullen PJ, Drøbak BK, Hanley MR, Dawson AP (1990) Thapsigargin, a tumor promoter, discharges intracellular Ca^{2+} stores by specific inhibition of the endoplasmic reticulum Ca^{2+}-ATPase. Proc Natl Acad Sci U S A 87:2466–2470.

Traynelis SF, Dingledine R (1989) Role of extracellular space in hyperosmotic suppression of potassium-induced electrographic seizures. J Neurophysiol 61:927–938.

Velumian AA, Carlen PL (1999) Differential control of three after-hyperpolarizations in rat hippocampal neurones by intracellular calcium buffering. J Physiol 517:201–216.

Verbalis JG (2003) Disorders of body water homeostasis. Best Pract Res Clin Endocrinol Metab 17:471–503.

Wang HS, Pan Z, Shi W, Brown BS, Wymore RS, Cohen IS, Dixon JE, McKinnon D (1998) KCNQ2 and KCNQ3 potassium channel subunits: molecular correlates of the M-channel. Science 282:1890–1893.

Williams ME, Washburn MS, Hans M, Urrutia A, Brust PF, Prodanovich P, Harpold MM, Stauderman KA (1999) Structure and functional charac-

terization of a novel human low-voltage activated calcium channel. J Neurochem 72:791–799.

Wittner L, Miles R (2007) Factors defining a pacemaker region for synchrony in the hippocampus. J Physiol 584:867–883.

Yaari Y, Beck H (2002) "Epileptic neurons" in temporal lobe epilepsy. Brain Pathol 12:234–239.

Yaari Y, Yue C, Su H (2007) Recruitment of apical dendritic T-type Ca^{2+} channels by backpropagating spikes underlies de novo intrinsic bursting in hippocampal epileptogenesis. J Physiol 580:435–450.

Yue C, Yaari Y (2004) KCNQ/M channels control spike afterdepolarization and burst generation in hippocampal neurons. J Neurosci 24:4614–4624.

Yue C, Yaari Y (2006) Axo-somatic and apical dendritic Kv7/M channels differentially regulate the intrinsic excitability of adult rat CA1 pyramidal cells. J Neurophysiol 95:3480–3495.

Yue C, Remy S, Su H, Beck H, Yaari Y (2005) Proximal persistent Na^+ channels drive spike afterdepolarizations and associated bursting in adult CA1 pyramidal cells. J Neurosci 25:9704–9720.

Yus-Najera E, Santana-Castro I, Villarroel A (2002) The identification and characterization of a noncontinuous calmodulin-binding site in noninactivating voltage-dependent KCNQ potassium channels. J Biol Chem 277:28545–28553.

Zhang Z, Bourque CW (2003) Osmometry in osmosensory neurons. Nat Neurosci 6:1021–1022.